J. Biomedical Science and Engineering, 2016, 9, 41-100
Published Online January 2016 in SciRes. http://www.scirp.org/journal/jbise
http://dx.doi.org/10.4236/jbise.2016.91005

Scientific Research Publishing

Homology Model and Ligand Binding Interactions of the Extracellular Domain of the Human $\alpha 4\beta 2$ Nicotinic Acetylcholine Receptor

Shu Mao[1,2], Hui Wen Ng[1], Michael Orr[3], Heng Luo[4], Hao Ye[1], Weigong Ge[1], Weida Tong[1], Huixiao Hong[1*]

[1]Division of Bioinformatics and Biostatistics, National Center for Toxicological Research, U.S. Food and Drug Administration, Jefferson, AR, USA
[2]School of Pharmacy and Bioengineering, Chongqing University of Technology, Chongqing, China
[3]Division of Nonclinical Science, Office of Science, Center for Tobacco Products, U.S. Food and Drug Administration, Silver Spring, MD, USA
[4]Division of Systems Biology, National Center for Toxicological Research, U.S. Food and Drug Administration, Jefferson, AR, USA
Email: *huixiao.hong@fda.hhs.gov

Received 5 November 2015; accepted 24 January 2016; published 28 January 2016

Abstract

Addiction to nicotine, and possibly other tobacco constituents, is a major factor that contributes to the difficulties smokers face when attempting to quit smoking. Amongst the various subtypes of nicotinic acetylcholine receptors (nAChRs), the $\alpha 4\beta 2$ subtype plays an important role in mediating the addiction process. The characterization of human $\alpha 4\beta 2$-ligand binding interactions provides a molecular framework for understanding ligand-receptor interactions, rendering insights into mechanisms of nicotine addiction and may furnish a tool for efficiently identifying ligands that can bind the nicotine receptor. Therefore, we constructed a homology model of human $\alpha 4\beta 2$ nAChR and performed molecular docking and molecular dynamics (MD) simulations to elucidate the potential human $\alpha 4\beta 2$-ligand binding modes for eleven compounds known to bind to this receptor. Residues V96, L97 and F151 of the $\alpha 4$ subunit and L111, F119 and F121 of the $\beta 2$ subunit were found to be involved in hydrophobic interactions while residues S153 and W154 of the $\alpha 4$ subunit were involved in the formation of hydrogen bonds between the receptor and respective ligands. The homology model and its eleven ligand-bound structures will be used to develop a virtual screening program for identifying tobacco constituents that are potentially addictive.

*Corresponding author.

How to cite this paper: Mao, S., Ng, H.W., Orr, M., Luo, H., Ye, H., Ge, W., Tong, W. and Hong, H. (2016) Homology Model and Ligand Binding Interactions of the Extracellular Domain of the Human $\alpha 4\beta 2$ Nicotinic Acetylcholine Receptor. *J. Biomedical Science and Engineering*, **9**, 41-100. http://dx.doi.org/10.4236/jbise.2016.91005

Keywords

Nicotinic Acetylcholine Receptors, Homology Model, Ligand-Receptor Interactions

1. Introduction

Most smokers continue tobacco use because of their nicotine addiction despite of the well-known adverse health consequences. Of the more than 40 million smokers in the United States, more than 70% of smokers express a desire to quit smoking [1]. Only 3% of smokers who made a quit attempt in the past year were successful [2] [3].

Nicotine from inhaled smoke rapidly moves into the brain to exert its actions by binding to neuronal nicotinic acetylcholine receptors (nAChRs), which are members of the Cys-loop family of ligand-gated ion channels [4]. To date, 12 neuronal-type nAChR subunits (α2-α10, β2-β4) which can assemble into functional heteromeric or homomeric (α-subunit only) pentamers have been identified [4]-[6]. In the mammalian brain, the $\alpha4\beta2$ subtypeisone of the most commonly found nAChRs [7] [8]. It plays important roles in mediating the nicotine reward and addiction process and has been targeted for nicotine addiction treatment [9]. The pocket of $\alpha4\beta2$ nAChR, to which various ligands can bind, is situated at the interface of the primary α4 subunit and the complementary β2 subunit [10] [11]. Understanding the molecular interactions between $\alpha4\beta2$ nAChR and its ligands could assist development of virtual screening of tobacco constituents with addiction potential through human $\alpha4\beta2$ nAChR binding. The three-dimensional (3D) structure of the receptor and its dynamic molecular properties are the key for elucidation of the molecular interactions [12]. However, the 3D structure of a human $\alpha4\beta2$ nAChR has yet to be experimentally determined. On the other hand, the 3D crystal structures of acetylcholine binding proteins (AChBPs) from *Lymnaea stagnalis* (Ls) [13], *Aplysia californica* (Ac) [14], and annelid *Capitella teleta* (Ct) have been experimentally determined [15] [16]. These AChBPs are structurally similar to the extracellular ligand-binding domain (LBD) of human AChRs and thus serve as an important surrogate for the study of nAChRs. Based on the template of these AChBP X-ray structures, homology structures of the human $\alpha4\beta2$ receptor have previously been constructed using the 3D crystal structure data for the AChBPs [11] [17] [18], although this information has not been made available to the scientific community.

In this study, we constructed a 3D homology model of the extracellular domain of the human $\alpha4\beta2$ nAChR (hereafter referred to as human $\alpha4\beta2$ nAChR) using the X-ray crystal structure of Ct-AChBP that was determined at a high resolution [19]. The homology structure of human $\alpha4\beta2$ nAChR was then further optimized using molecular dynamics (MD) simulations through the exploration of the accessible structural space for the complex [20] [21]. We used the eleven compounds (including compounds contained in tobacco products such as nicotine) that were co-crystalized with nAChRs or AChBPs to elucidate the ligand binding interactions because there are $\alpha4\beta2$ binding data for these eleven compounds. These eleven $\alpha4\beta2$-ligand complex structures were obtained from molecular docking and further optimized by MD simulations. Examining the binding modes of these compounds in the $\alpha4\beta2$ nAChR homology model revealed that hydrophobic interactions between ligands and V96, L97 and F151 of the α4 subunit and L111, F119 and F121 of the β2 subunit and the hydrogen bonds with S153 and W154 of the α4 subunit played key roles for the ligand binding.

The 3D structures of our human $\alpha4\beta2$ nAChR homology model, its eleven ligand-bound complexes (supplementary materials which were made publically available), and the elucidated key interactions of these ligands in the $\alpha4\beta2$binding pocket, could be used to develop a model for rapid screening of tobacco constituents with addiction potential through human $\alpha4\beta2$ nAChR binding.

2. Material and Methods

2.1. Study Design and Workflow

The study design and workflow were shown in **Figure 1.** Briefly, the human $\alpha4\beta2$ nAChR (target) sequences were first searched in the PDB using BLAST to select a highly homologous protein (template). The 3D structure of human $\alpha4\beta2$ nAChR was then built using homology modeling. After docking the ligand co-crystalized with the template protein, the initial $\alpha4\beta2$-ligand complex was then optimized with MD simulations. After MD optimization, the ligand was removed from the complex. The remaining optimized 3D structure of human $\alpha4\beta2$

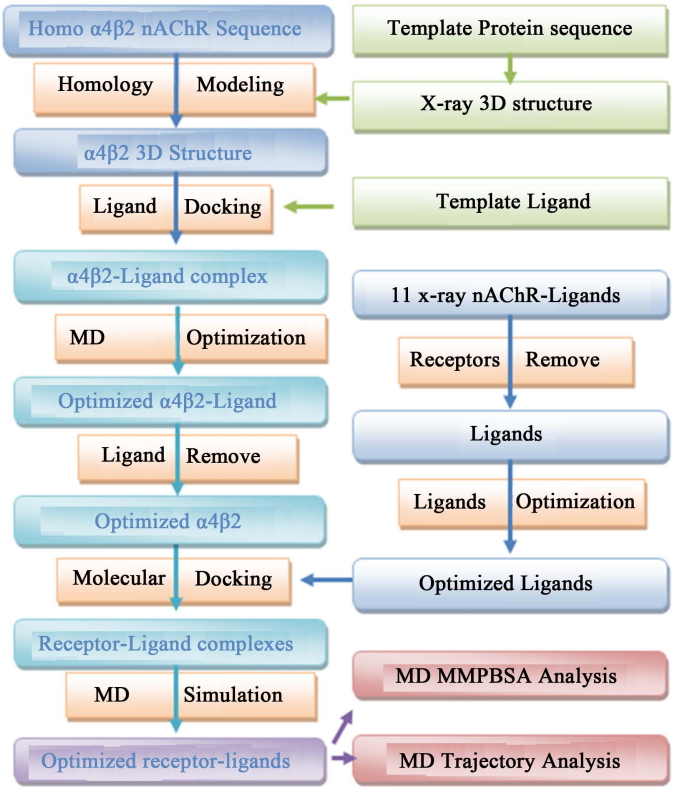

Figure 1. Study design and overall workflow. BLAST was used to search the human $\alpha 4\beta 2$ nAChR sequence against PDB to select a template sequence for homology modeling. The initial homology model was then optimized using MD simulations. Eleven structurally diverse ligands PDB were docked into the optimized$\alpha 4\beta 2$ and followed by MD simulations.

nAChR was used to define a binding grid for subsequent docking analyses. Eleven structurally diverse $\alpha 4\beta 2$ ligands were selected from PDB database and their 3D structures were built and optimized. The optimized ligands were then docked into the $\alpha 4\beta 2$ binding pocket. The $\alpha 4\beta 2$-ligand complexes obtained from docking were further optimized through MD simulations. Finally, the protein-ligand interactions were analyzed by examining the trajectory of MD simulations.

2.2. Homology Modeling

The tertiary structure of a protein is better conserved than its amino acid sequence [22] [23]. Homology modeling is widely used to construct atomic-resolution models for proteins without experimentally determined structures from their amino acid sequences and experimental 3D structures of related homologous proteins [12] [24]. The homology model of human $\alpha 4\beta 2$ nAChR was built using Maestro 9.6 in the Schrödinger Suite [25]. The extracellular ligand-binding domain sequences of the human $\alpha 4$and $\beta 2$ nAChR subunits were downloaded from UniProt database [26] ($\alpha 4$: P43681(29-242), ACHA4_HUMAN and $\beta 2$: P17787(26-233), ACHB2_HUMAN). The 3D structure of Ct-AChBPs (UniprotID: I6L8L2) was downloaded from PDB (PDB ID: 4AFH) [19] as the template structure. The template sequence was identified through searching the target human $\alpha 4\beta 2$ sequences in PDB using the BLAST homology searching with default parameters in the Prime 3.4. The target and the template sequences were aligned using the ClustralW method employed in Prime 3.4. The hetero-multimer model was used to predict the secondary structure of human $\alpha 4\beta 2$ dimer. The ligand co-crystalized with the template protein was removed before homology modeling.

2.3. Molecular Docking

There are many structure-activity relationship techniques such as pharmacophore modeling [27]-[29], comparative molecular field analysis [30] [31], machine learning methods [32] such as classification tree model [33] and

Decision Forest models [34]-[41] based on molecular descriptors [42] that are calculated using the algorithm developed for the expert systems of structure elucidation [43]-[49], and molecular docking [15] [50] [51]. Molecular docking was used in our previous studies of interactions between ligands and estrogen receptors [52] [53] for prediction of estrogenic activity [54] and endocrine disruptions [53] [55]. A similar docking protocol was adopted in this study. The 3D structure of $\alpha 4\beta 2$ nAChR obtained from homology modeling followed by MD optimizations was prepared using the "protein preparation" tool in the Schrödinger suite [25]. The protein structures were optimized to reach the converged RMSD of 0.3 angstrom (Å) under OPLS_2005 force field. The grid box was defined using "receptor Grid Generation" tool also in the Schrödinger suite. The grid was set as a 15 × 15 × 15 (x × y × z, Å) cubic box around the ligand thus comprising the entire binding pocket.

The two-dimensional (2D) structures of the eleven compounds co-crystalized with AChBPs in PDB are shown in **Figure 2**. Hereafter, the 3-letter symbols given in **Figure 2** will be used to indicate the ligands for simplicity; their names and experimental activity data are also given in Supplementary **Table S1**. Their 3D structures of the ligands were obtained from the corresponding PDB files of the bound AChBP complexes and further optimized usingLigPrep2.8 tool and OPLS_2005 force field in Schrödinger suite. Epik 2.6 tool of Schrödinger suite was used to generate the ligands ionization states at pH 7.0 ± 2.0. The optimized ligands were docked into the docking grid in the 3D structure of $\alpha 4\beta 2$ using Glide 6.1 tool in the Schrödinger suite with standard precision (SP). The binding poses with the top glide scores were selected and the corresponding complexes were output for subsequent MD simulations.

2.4. MD Simulations

The 3D structure of the human $\alpha 4\beta 2$ homology model and the eleven$\alpha 4\beta 2$-ligand complexes output from molecular docking were optimized using MD simulations. The MD simulations were carried out through AMBER11 [56] using the Amber ff99SB force field [57] and general Amber force field (GAFF) [58] for the receptor and ligands, respectively. AM1-BCC charges [59] were added for the ligands using Antechamber. The topology and parameters of the complexes were constructed by LEAP program [56]. Each complex was solvated with TIP3P water molecules with a 10.0 Å truncated octahedron periodic box. Sodium ions were added to maintain charge neutrality of the systems. The SHAKE algorithm [60] was used to constrain the bonds involving hydrogen. The Particle-mesh Ewald (PME) algorithm [61] was used to deal with the long-range interactions with a 8.0 Å non-bonded interactions cutoff. Prior to MD production simulations, a total of 10,000 steps of minimizations were applied to the entire model system including solvent molecules, followed by 2000 steps of steepest-descent, and subsequently 8000 steps of conjugated gradient minimizations. Two hundred ps (picoseconds) of equilibrations were applied to the system to reach the stable state. The molecular systems were heated in NVT ensemble from 0 to 300 K gradually over 200 ps with weak harmonic potential solutes restrained. After equilibration, 50 and 10 ns (nanoseconds) NPT ensemble MD simulations were performed for the $\alpha 4\beta 2$ homology model and its eleven ligand-bound complexes, respectively, at 1 atm pressure, temperature of 300 K and a time step of 2 fs (fem to seconds). The coordinates of the systems were saved every 10 ps for subsequent trajectory analyses.

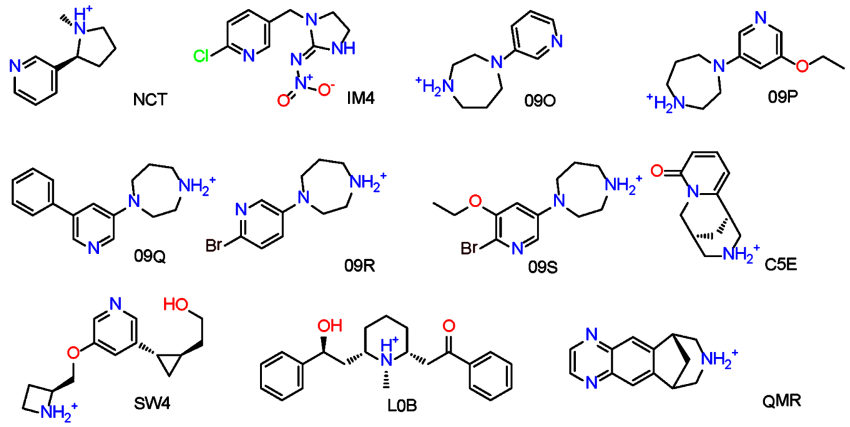

Figure 2. Chemical structures of the eleven compounds in the AChBPs complexes collected from PDB and their names used in this paper.

3. Results and Discussion

3.1. Optimized 3D Structure of Human $\alpha 4\beta 2$ nAChR Homology Model

The sequences of the $\alpha 4$ and $\beta 2$ subunits of the human nAChRs were queried using the BLAST algorithm to select a template structure in the protein data bank (PDB) to be used for the homology modeling of the human $\alpha 4\beta 2$ nAChR. The $\alpha 4$ subunit sequence was aligned with 811 sequences in PDB (see Supplementary **Table S2**). The $\beta 2$ subunit sequence was aligned with 765 sequences in PDB (see Supplementary **Table S3**). Recent studies have demonstrated that 3D structures can be constructed using homology modeling based on template structures of proteins with 25% or higher sequence identity to the target proteins [62] [63]. The 3D structure of marine annelid Ct-AChBP with PDB ID 4B5D at a resolution of 2.2 Å has been successfully used previously as the template for the homology modeling of $\alpha 4\beta 2$ nAChR to study the structural determinants of ligand recognition in-human $\alpha 4\beta 2$nAChR [11]. The crystal structure of Ct-AChBP with a higher resolution of 1.88 Å had been determined recently and deposited in PDB (ID: 4AFH). The $\alpha 4$ and $\beta 2$ subunit sequences were found to have 31% and 28% sequence identities, respectively, with the 4AFH structure. Therefore, this was used as the template to construct the homology model of the human $\alpha 4\beta 2$ nAChR.

The final alignment between the template and the target with the secondary structure prediction is shown in **Figure 3** (the first three residues of $\alpha 4$ subunit were not included in the homology modeling because they could not be aligned to the template sequence).Most of the secondary structures including the disulphide bridges aligned well between the template and the target. The core residues located at the dimer interface, include residues Y98, W154 and Y195from the $\alpha 4$ subunit and residues W57, V111, F119 and L121 from the$\beta 2$ subunit. These core residues played key roles in $\alpha 4\beta 2$-ligand interactions, which is consistent with the interactions between the human $\alpha 4\beta 2$ nAChR and the nicotine addiction treatment drug varenicline derived from analysis using the structure-guided mutagenesis [19].

The 3D structure of the human $\alpha 4\beta 2$ dimer shown in **Figure 4(a)** was constructed by homology modeling using the structure of Ct-AChBP (**Figure 4(b)**) as the template. The homology model superimposed well with the template structure as depicted in **Figure 4(c)**. Consistent with our expectation, the α helices and β sheets in both the template and target structures were more conserved compared to the loops. Our homology model was

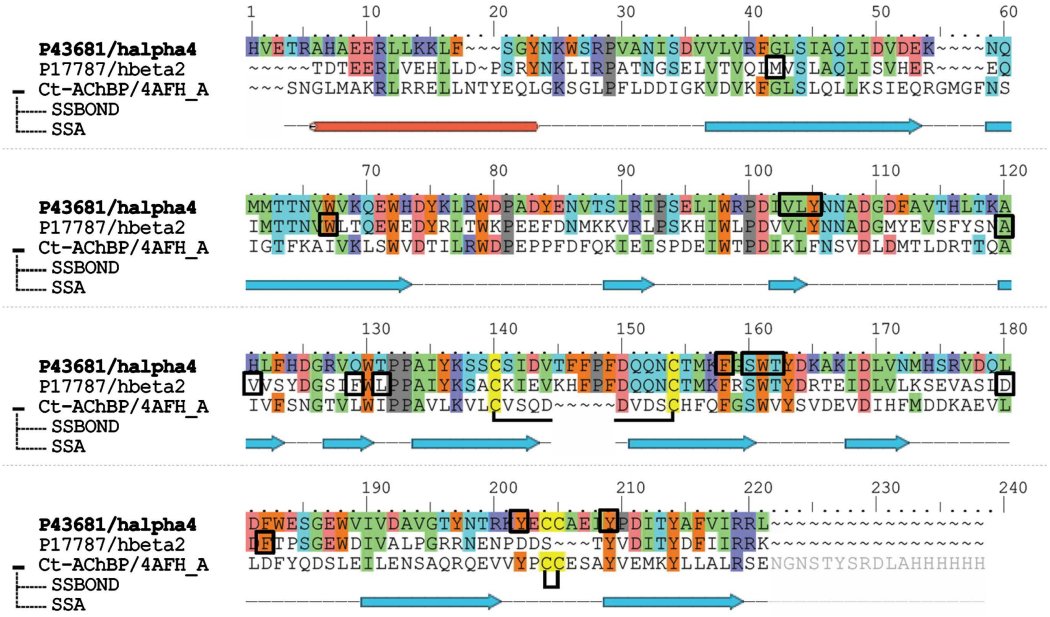

Figure 3. Sequence alignment result between the human $\alpha 4\beta 2$ nAChR and the template Ct-AChBP. The predicted secondary structure from Ct-AChBP is also shown: the tube represents the helix; arrows indicate strands; and dotted lines depict loops. The identical residues are highlighted in colors according to the property of the corresponding query residue in the alignment to depict the location of charged (purple: positive charge; red: negative charge), aromatics (brown), polar (cyan), hydrophobic (green) and special (yellow: cysteine; grey: proline) query residues. The residues that interact with the ligands are marked with black boxes.

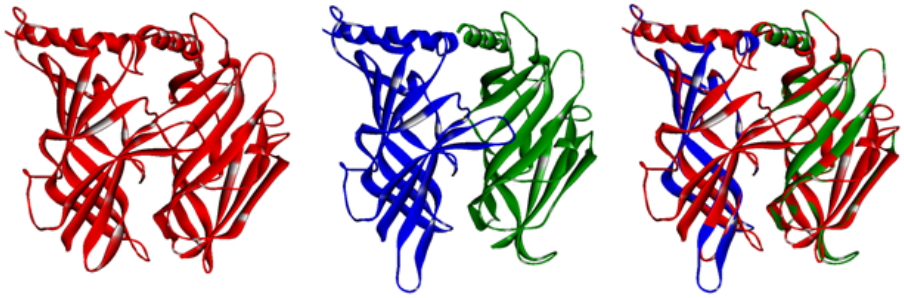

(a) (b) (c)

Figure 4. Homology model of the human $\alpha 4\beta 2$ nAChR. Template structure Ct-AChBP color coded in red (a) and the homology model is shown in solid blue ribbons for $\alpha 4$ and green ribbons for $\beta 2$ (b). Superimposition of the homology model with the template is depicted in (c).

compared with the homology model constructed using a template structure of the same protein with a slightly lower resolution [11]. The overall structure and key structural features were similar.

More often than not, initial 3D structures from homology modeling were further optimized using MD simulations [64]. MD simulations are a technique widely applied to study protein folding, protein dynamics and protein-ligand interactions [20] [21] [65]-[69]. Considering the ligand impact on the residues conformations in the binding pocket [20] of the $\alpha 4\beta 2$ homology model, MD simulations were performed in the presence of the ligand (LOB) (co-crystallized in the Ct-AChBP template protein). The root mean square deviation (RMSD) values of the optimized human $\alpha 4\beta 2$-LOB complex structure were calculated to characterize the dynamic property of the molecular system during the MD simulations and were plotted in **Figure 5(a)**. The molecular system reached stable states during the 50 ns simulations. The RSMD value of human $\alpha 4\beta 2$ backbone atoms was stabilized at 3.5 Å after 30 ns simulations and the ligand fluctuated stably from 43 ns with a RMSD of 2.0 Å. The optimized human $\alpha 4\beta 2$ homology model is available upon request.

The root-mean-square fluctuations (RMSF) of residues of the human $\alpha 4\beta 2$ homology model during the MD simulations were calculated to characterize the mobility of the individual residues and plotted in **Figure 5(b)**. As expected, the N-terminal alpha helix and the 10 beta strands are more rigid than the loops and, thus, had smaller RMSF values. The peaks in **Figure 5(b)** indicated larger RMSF values for the residues in the loops: 130 - 140, 170 - 180, 260 - 270, 280 - 290, 340 - 350 and 400 - 410.

The Ramachandran plot (**Figure 5(c)**) showed that 99.3% of the residues in the optimized $\alpha 4\beta 2$ structure were in the favorable regions-higher than the percentage of residues (96.2%, see **Figure 5(d)**) in the initial homology model without MD simulations—thus indicating that the homology model of human $\alpha 4\beta 2$ was optimized to an energy stable state.

To examine the structural changes of the $\alpha 4\beta 2$ homology model following the MD simulations, the structures before and after the optimization were superimposed together and depicted in **Figure 5(e)**. The two structures superimposed well with each other, especially for the β-sandwich cores, providing evidence that the homology model is a reasonably stable structure. On the other hand, much larger changes in the loop regions (some near the ligand binding site) were observed during the simulations points towards a better characterized ligand binding pocket for the $\alpha 4\beta 2$. This indicates that optimization using MD simulations is a necessary step for the structural refinement of the human $\alpha 4\beta 2$ homology model.

To examine the binding interactions between the human $\alpha 4\beta 2$ homology model and the cognate ligand in the template, LOB, the zoomed-in view of the receptor ligand binding pocket is shown in **Figure 5(f)**. The tertiary amine of LOB was stabilized through the π-cation interactions with the conserved aromatic residues W154 and Y195. The benzene ring of LOB also interacted with the piperidine ring of residue W154through π-π interactions. The receptor-ligand hydrophobic interactions mainly involved residues V96 and L97 from the $\alpha 4$ subunit and V111, F119 and L121 from the $\beta 2$ subunit. The binding interactions observed for the human $\alpha 4\beta 2$ homology model were similar to those between LOB and Ct-AChBP elucidated from the X-ray structure [19].

3.2. Ligands Docking

Site Map [70] was used to generate the potential ligand binding site of the extracellular domains of human

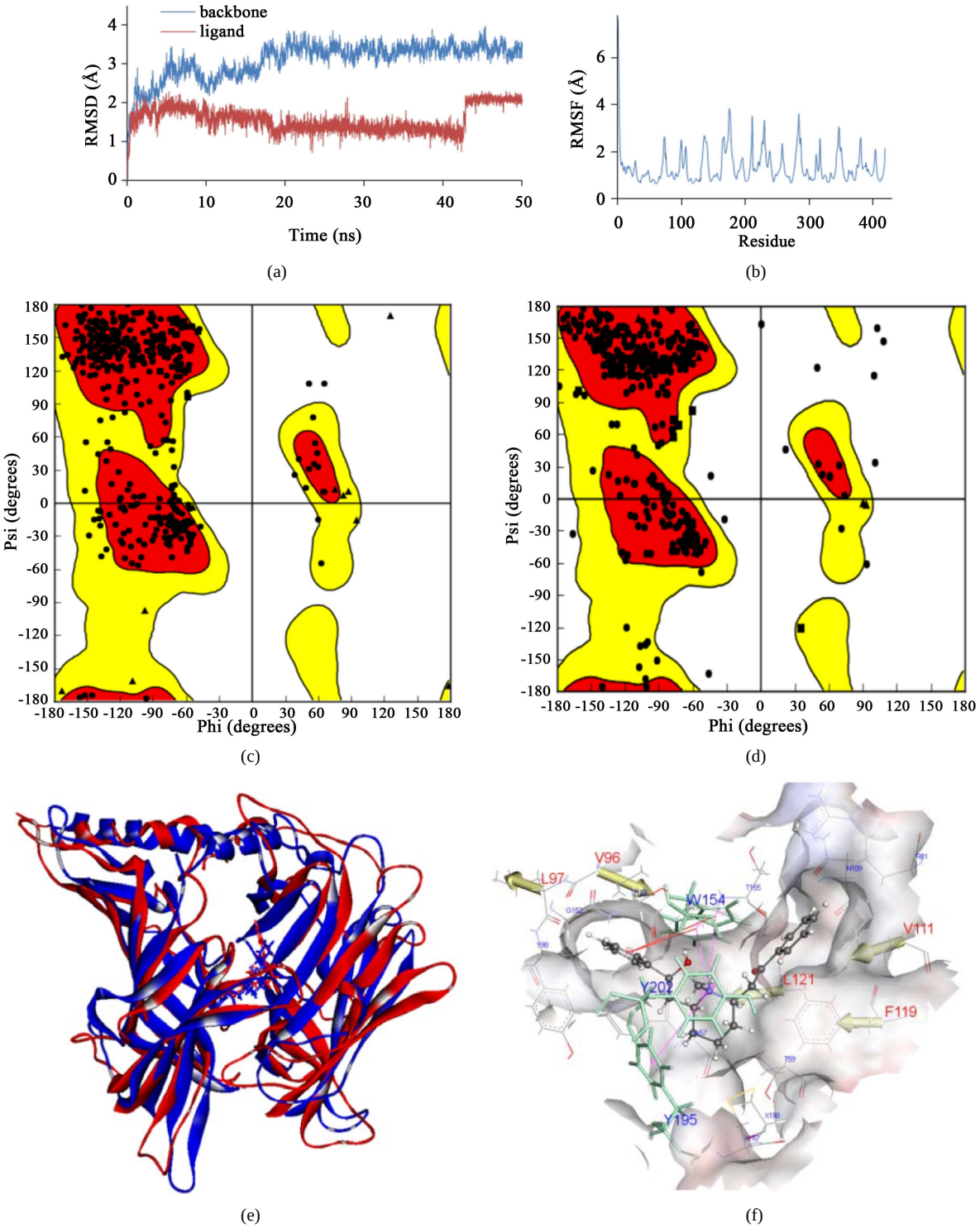

Figure 5. Optimization of the homology model by MD simulations. The RMSD values (y-axis) for atoms of protein backbone (blue line) and ligand (red line) during the optimization (x-axis) were plotted in (a). The RMSF values (y-axis) of individual residues (x-axis) were given in (b). Ramachandran plots of the optimized and initial homology models were given in (c) and (d), respectively. The homology models before (blue ribbon) and after (red ribbon) the MD simulations were superimposed (e). The binding pocket was illustrated by a zoomed surface representation (f). The core residues were color coded in blue. The arrows indicated the hydrophobic moment (residues colored in red). The red lines depicted the π-π interaction and the purple lines for the π-cation interaction.

$\alpha 4\beta 2$n AChR homology model. The eleven ligands shown in **Figure 2** were docked in the receptor model. For each ligand, the lowest docking score and its corresponding docking pose in the receptor were selected and output for subsequent analysis. The docking poses of all eleven ligands in the human $\alpha 4\beta 2$ nAChR homology model are shown in **Figure 6** and Supplementary **Figure S1**. The ligand binding site composed of the $\alpha 4$ subunit residues V96, L97, Y98, S153, W154, Y195 and Y202 and the $\beta 2$ subunit residues W57, V111, F119, L121 and F157. The orientations of the eleven ligands were similar *i.e.* the hydrophobic parts of all the ligands extended into the major surface of the binding pocket. Aromatic and hydrophobic interactions were the major contributions to the binding.

3.3. Ligand Binding Interactions

To elucidate the binding modes of the eleven ligands in the human $\alpha 4\beta 2$ receptor, the complexes of $\alpha 4\beta 2$ bound with the ligands resulting from the molecular docking were again optimized using MD simulations [71] [72]. MD simulations were carried out on the eleven human $\alpha 4\beta 2$-ligand complexes obtained from molecular docking and the results were given in **Figure 7**. The RMSD values generated by the MD simulations for the proteins (**Figure 7(a)**) and the ligands (**Figure 7(b)**) indicated the complexes reached relatively stable states. In more detail, for the structures of $\alpha 4\beta 2$ homology model bound with IM4, 09O, 09R, LOB and QMR ligands, the irreceptor RMSD values stabilized around 2.0 Å after 6 ns MD simulations. On the other hand, the structures of $\alpha 4\beta 2$ homology model bound with NCT, 09P, 09Q, 09S, SW4 and C5E continued to show small fluctuations of the receptor (RMSD values of ~2.5 Å) after 6 ns MD simulations. Furthermore, as expected, the rigid ligands (C5E and QMR) remained highly stable as evidenced by a low RMSD of 0.3 Å during the whole simulations; the ligands with one rotatable bond (NCT and 09R) had slightly larger fluctuations of ~1 Å RMSD; the ligands with multiple rotatable bonds (e.g. 09Q, 09S, and SW4) had larger fluctuations in the simulations. In other words, the more rotatable bonds in a ligand, the larger the RMSD. Interestingly, LOB has six rotatable bonds but its conformation only changed slightly with RMSD values of about 0.5 Å during the simulations. This indicates that the fluctuation of a ligand in simulations depends not only on the ligand structure but also on its binding environment [73] [74].

To elucidate the binding interactions of the eleven ligands, the corresponding receptor-ligand complexes from the final frame of the MD simulations were examined. The binding mode of NCT was shown in **Figure 8(a)**. On the $\alpha 4$ subunit side, NCT had extensive binding with residues Y98, S153, W154 and Y202 through hydrogen bond, π-π and π-cation interactions. It also bound with the hydrophobic residues V96, L97 and F151 through hydrophobic interactions. On the $\beta 2$ subunit side, the ligand bound with W57 and L121 through π-sigma interactions and hydrophobic interactions. The receptor-ligand interactions observed for the human $\alpha 4\beta 2$ nAChR are consistent with the ones found in AChBP crystal complex of the same ligand [72].

The binding interactions between $\alpha 4\beta 2$ and IM4 were shown in **Figure 8(b)**. The pyridine ring of IM4 interacted with $\alpha 4\beta 2$ through the π-π interactions with residue Y195 of the $\alpha 4$ subunit and the hydrophobic interact-

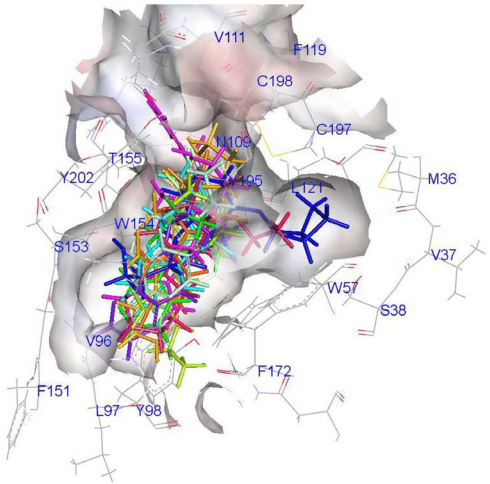

Figure 6. Docking poses of the eleven ligands in the binding site of human $\alpha 4\beta 2$.

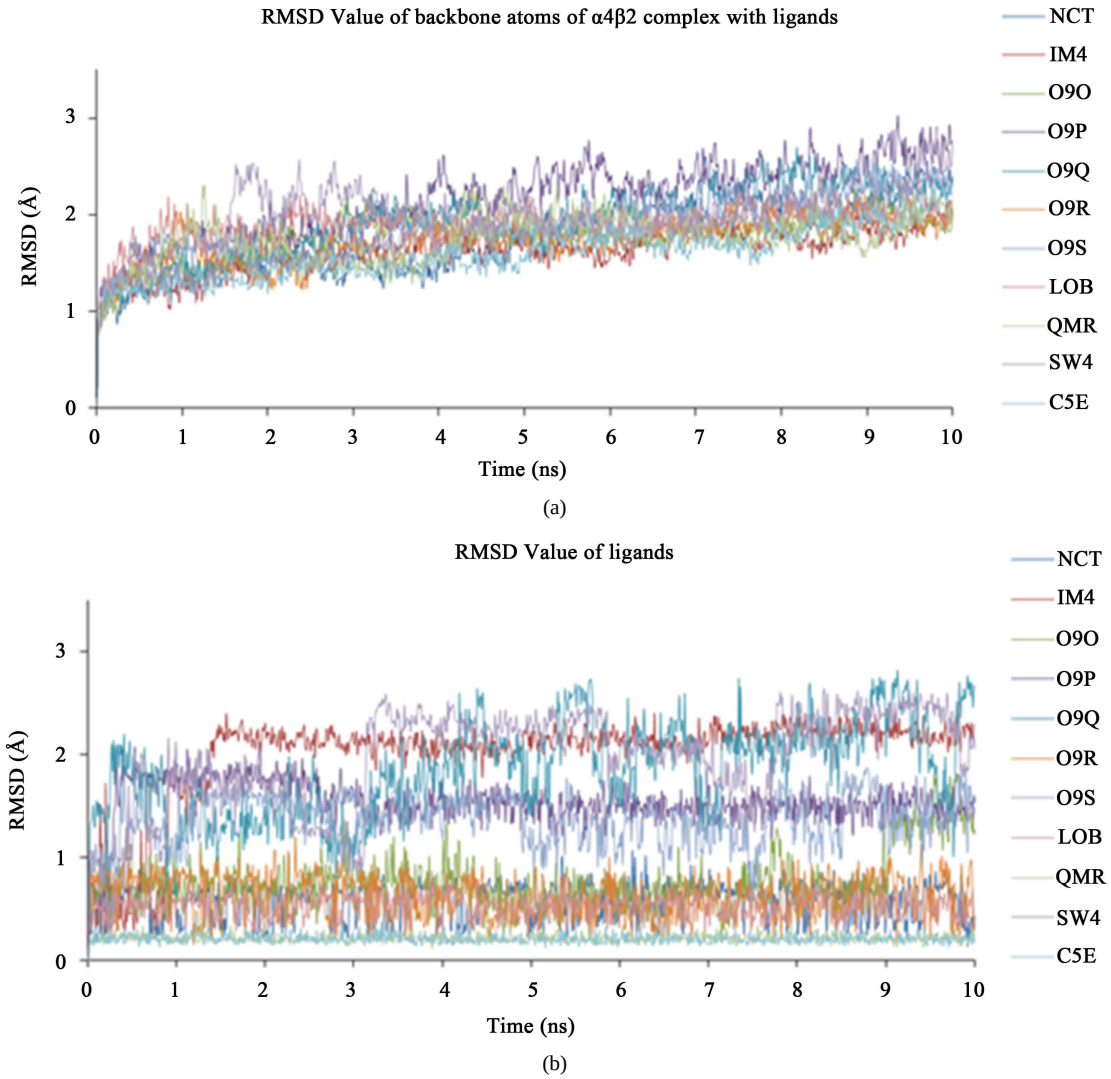

Figure 7. Trajectory analyses of MD simulations. The RMSD values of the protein backbones (a) and the ligands (b) were plotted again the time. The complexes are indicated by the ligand abbreviations using different colors shown in the legends.

tions with residues L111, L119 and F172 of the β2 subunit. The binding mode of IM4 in the human α4β2 elucidated in this study was similar to the one observed in the crystal structure of the Ls-AChBP complex bound with IM4 [74].

Ligands 09O, 09P, 09Q, 09R and 09S share a structural fragment in which a diazepane and a pyridine are connected by a single bond. Their binding interactions with the human α4β2 homology model are depicted in **Figures 8(c)-(g)**, respectively. Although the binding modes of these ligands in the receptor were not the same due to the structural elements attached to the common fragment, the binding interactions formed were similar. These interactions were hydrogen bond, hydrophobic, π-π and π-cation interactions. The π-π and π-cation interactions mainly occurred between the diazepane and pyridine of the ligands and the residues W154, Y195, Y202, V96, L97 and Y98 of the α4 subunit and the residues W57, L121, F172 and F119 of the β2 subunit. These binding interactions as elucidated from our MD simulations are consistent with the ones identified in the AChBP X-ray complex structures bound with the respective ligands [75].

The ligand binding mode ofSW4is illustrated in **Figure 8(h)**. SW4 forms a hydrogen bond with residue Y196 of the α4 subunit and had π-cation and hydrophobic interactions with residues V111, F119 and F121 of the β2 subunit. These binding interactions were observed in the x-ray crystal structure of the Ct-AChBP bound with SW4 [11].

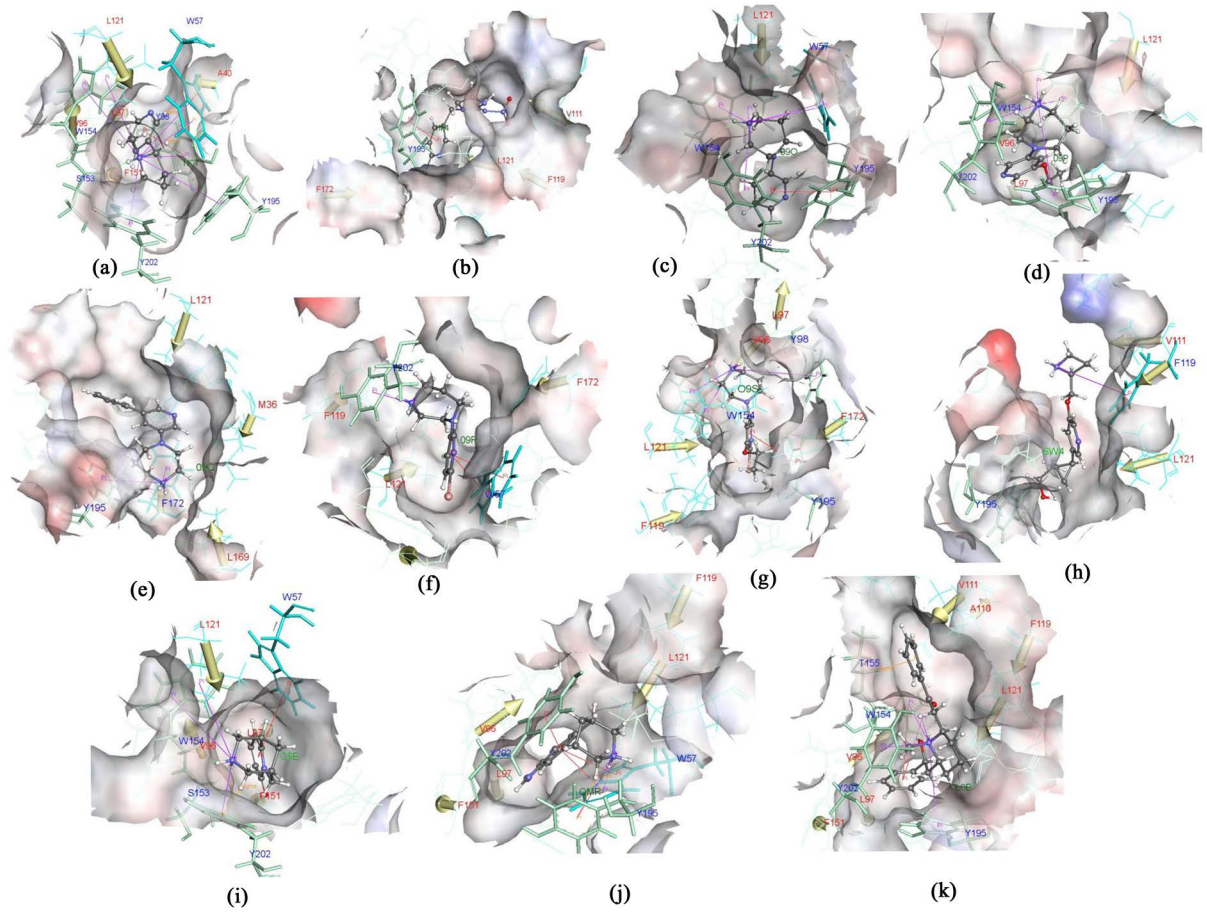

Figure 8. Ligands binding modes. Binding pocket surfaces are colored in the interpolated charge. The core residues are in cyan and the arrows indicated the hydrophobic moments (residues were labelled in red).The red lines depicted the π-π interaction and the purple lines for the π-cation interaction. The ligands in the complexes: NCT (a); IM4 (b); 09O (c); 09P (d); 09Q (e); 09R (f); 09S (g); LOB (h); QMR (i); SW4 (j) and C5E (k).

Figure 8(i) depicts the binding mode ofC5E.The ligand bound with the human $\alpha 4\beta 2$ through hydrogen bonds, π-cation interactions, π-sigma interactions and hydrophobic interactions with the residues V96, L97, F151, S153, W154 and Y202 of the $\alpha 4$ subunit. It also has π-π interactions and hydrophobic interactions with the residues W57 and L121 of the $\beta 2$ subunit. The binding interaction was confirmed in the x-ray structure of Ac-AChBP complex bound with C5E [76].

The binding mode of QMR is shown in **Figure 8(j)**. This highly rigid ligand bound to the binding pocket through π-π interactions, π-cation interactions, π-sigma interactions and hydrophobic interactions with residues V96, L97, F151, Y195 and Y202 of the $\alpha 4$ subunit and the side chains of residues W57, F119 and F121 of the $\beta 2$ subunit. These binding interactions were in a good agreement with the Ac-AChBP complex bound with the same ligand [76].

The binding mode of LOB is given in **Figure 8(k)**. LOB interacted with $\alpha 4\beta 2$ through π-cation interactions with residues W154, Y195 and Y202 and π-π interactions with W154 of the $\alpha 4$ subunit. It also had hydrophobic interactions with residues V96, L97 and F151 of the $\alpha 4$ subunit and residues V111, F119 and L121of the $\beta 2$ subunit. These molecular interactions were similar to those observed in x-ray structure of LOB-CtAChBP complex [19].

The binding interactions between the human $\alpha 4\beta 2$ homology model and the eleven ligands were summarized in the **Table 1**. In general, the hydrophobic interactions mainly involved residues V96, L97 and F151 of the $\alpha 4$ subunit and residues L111, F119 and F121 of the $\beta 2$ subunit. The π-π, π-cation, and π-sigma interactions were mainly from residues Y98, W154, Y195 and Y202 of the $\alpha 4$ subunit and from residue W57 of the $\beta 2$ subunit.

Table 1. Summary of predicted binding interactions.

Ligand	Name	H Bond	pi-pi	Pi-Cation	Pi-Sigma	Hydrophobic
NCT	L-(-)-nicotine	NCT:H15-S153:O	Y98-NCT	Y98, W154, Y202-NCT:N2	W57-NCT:H1, H5	V96, L97, F151, L121
IM4	Imidacloprid		Y195-IM4			V111, F119, F172
09O	1-(pyridin-3-yl)-1,4-diazepane	09O:H5-W154:O	Y195-09O	W154-09O:N1 W57-09O:N1		L121
09P	1-(5-ethoxypyridin-3-yl)-1,4-diazepane	09P:H3-W154:O		W154, Y195, Y202-09P:N1		V96, L97, L121
09Q	1-(5-phenylpyridin-3-yl)-1,4-diazepane			Y195-09Q:N2 F172-09Q:N2		M36, L121, L169, F172
09R	1-(6-bromopyridin-3-yl)-1,4-diazepane		W57-09R	Y202-09R:N3		V96, F119, L121, F172
09S	1-(6-bromo-5-ethoxypyridin-3-yl) -1,4-diazepane	Y195:HH-09S:N3	Y195-09S	Y98, W154-09S:N1		V96, L97, F119, L121, F172
LOB	Alpha-lobeline		W154-LOB	W154, Y195, Y202-LOB:N1	LOB-T155:HA	V96, L97, F151, A110, V11, F119, L121
QMR	Varenicline		Y202-QMR W57-QMR	Y195-QMR:N1 W57-QMR:N1	Y195-QMR:H1	V96, L97, F15, F119, L121
SW4	2-[(1R,2S)-2-[5-[[(2S)-azetidin-2-yl] methoxy]pyridin- 3-yl]cyclopropyl]ethanol	Y195:HH-SW4:O1		F119-SW4:N2		V111, F119, F121
C5E	Cytisine	C5E:H6-S153:O; C5E:H15-W154:O	W57-C5E	W154, Y202-C5E:N2	Y202-C5E:H4	V96, L97, F151, L121

The hydrogen bonds were formed between the ligands and residues S153 and W154 of theα4 subunit. It is worth noting that residues W154 and W57 interacted with most of the eleven ligands and played key roles in the binding as confirmed in the X-ray structures of the AChBPs bound with the respective ligands [19] [77]. It is worth noting that in this study, we focus on the binding of these ligands to the human $\alpha4\beta2$ nAChR *i.e.* the pre-requisite step for chemicals to elicit subsequent pharmacological actions on the body-indeed, the ligands considered in this study display different pharmacology (various degree of activation and desensitization) upon binding to the human $\alpha4\beta2$ nAChR. However, this aspect is out of the scope of our study.

4. Conclusion

The human $\alpha4\beta2$ nAChR plays an important role in nicotine addiction and could be used for screening tobacco constituents with addiction potential. Determining the 3D structure of the human $\alpha4\beta2$ nAChR and elucidating its ligand binding interactions would help with screening for tobacco constituents with nicotine receptor binding activity and addictive properties. This type of screening will result in a rank order of tobacco constituents that have addiction potential and may inform regulation of tobacco products. As there are no 3D structures of human $\alpha4\beta2$ nAChR either alone or bound with ligands available to researchers today, we constructed a homology model of the human $\alpha4\beta2$ nAChR based on the X-ray structure of the Ct-AChBP complex bound with LOB as an alternative approach for gaining insights into ligand binding characteristics of the human $\alpha4\beta2$ nAChR. Based on the homology model of the human $\alpha4\beta2$ nAChR, we further characterized the ligand binding interactions of human $\alpha4\beta2$ nAChR by docking eleven ligands to the receptor followed by MD simulations. Our results provide molecular details into the ligand binding interactions with human $\alpha4\beta2$ nAChR homology model and a modeling method for identifying nicotine receptor binding compounds that are potentially addictive.

Acknowledgements

This project was funded by the Center for Tobacco Products at the U.S. Food and Drug Administration. This research was supported in part by an appointment to the Research Participation Program at the National Center for Toxicological Research (Hui Wen Ng and Hao Ye) administered by the Oak Ridge Institute for Science and Education through an interagency agreement between the U.S. Department of Energy and the U.S. Food and

Drug Administration. This publication represents the views of the author(s) and does not represent CTP position or policy.

Author Contributions

H.H. and M.O. conceived and designed the experiments; M.S. and H.W.N. performed the experiments; M.S., H.W.N., H.L., H.Y. and W.G. analyzed the data; M.S., M.S., W.T. and H.H. wrote the paper.

Conflicts of Interest

The authors declare no conflict of interest.

References

[1] Dube, S., Asman, K., Malarcher, A. and Carabollo, R. (2009) Cigarette Smoking among Adults and Trends in Smoking Cessation-United States, 2008. *Morbidity and Mortality Weekly Report*, **58**, 1227-1232.

[2] Benowitz, N.L. (2009) Pharmacology of Nicotine: Addiction, Smoking-Induced Disease, and Therapeutics. *Annual Review of Pharmacology and Toxicology*, **49**, 57-71. http://dx.doi.org/10.1146/annurev.pharmtox.48.113006.094742

[3] Benowitz, N.L. (2010) Nicotine Addiction. *New England Journal of Medicine*, **362**, 2295-2303. http://dx.doi.org/10.1056/NEJMra0809890

[4] Jensen, A.A., Frølund, B., Liljefors, T. and Krogsgaard-Larsen, P. (2005) Neuronal Nicotinic Acetylcholine Receptors: Structural Revelations, Target Identifications, and Therapeutic Inspirations. *Journal of Medicinal Chemistry*, **48**, 4705-4745. http://dx.doi.org/10.1021/jm040219e

[5] Dani, J.A. and Bertrand, D. (2007) Nicotinic Acetylcholine Receptors and Nicotinic Cholinergic Mechanisms of the Central Nervous System. *Annual Review of Pharmacology and Toxicology*, **47**, 699-729. http://dx.doi.org/10.1146/annurev.pharmtox.47.120505.105214

[6] Liu, X. (2014) Effects of Blockade of Alpha 4 Beta 2 and Alpha 7 Nicotinic Acetylcholine Receptors on Cue-Induced Reinstatement of Nicotine-Seeking Behaviour in Rats. *International Journal of Neuropsychopharmacology*, **17**, 105-116. http://dx.doi.org/10.1017/S1461145713000874

[7] Albuquerque, E.X., Pereira, E.F., Alkondon, M. and Rogers, S.W. (2009) Mammalian Nicotinic Acetylcholine Receptors: From Structure to Function. *Physiological Reviews*, **89**, 73-120. http://dx.doi.org/10.1152/physrev.00015.2008

[8] Millar, N.S. and Gotti, C. (2009) Diversity of Vertebrate Nicotinic Acetylcholine Receptors. *Neuropharmacology*, **56**, 237-246. http://dx.doi.org/10.1016/j.neuropharm.2008.07.041

[9] Miwa, J.M., Lester, H.A. and Walz, A. (2012) Optimizing Cholinergic Tone through Lynx Modulators of Nicotinic Receptors: Implications for Plasticity and Nicotine Addiction. *Physiology*, **27**, 187-199. http://dx.doi.org/10.1152/physiol.00002.2012

[10] Tapper, A.R., McKinney, S.L., Nashmi, R., Schwarz, J., Deshpande, P., Labarca, C., Whiteaker, P., Marks, M.J., Collins, A.C. and Lester, H.A. (2004) Nicotine Activation of Alpha4* Receptors: Sufficient for Reward, Tolerance, and Sensitization. *Science*, **306**, 1029-1032. http://dx.doi.org/10.1126/science.1099420

[11] Zhang, H.K., Eaton, J.B., Yu, L.F., Nys, M., Mazzolari, A., van Elk, R., Smit, A. B., Alexandrov, V., Hanania, T., Sabath, E., Fedolak, A., Brunner, D., Lukas, R.J., Vistoli, G., Ulens, C. and Kozikowski, A.P. (2012) Insights into the Structural Determinants Required for High-Affinity Binding of Chiral Cyclopropane-Containing Ligands to Alpha 4 Beta 2-Nicotinic Acetylcholine Receptors: An Integrated Approach to Behaviorally Active Nicotinic Ligands. *Journal of Medicinal Chemistry*, **55**, 8028-8037. http://dx.doi.org/10.1021/jm3008739

[12] Vernall, A.J., Stoddart, L.A., Briddon, S.J., Ng, H.W., Laughton, C.A., Doughty, S.W., Hill, S.J. and Kellam, B. (2013) Conversion of a Non-Selective Adenosine Receptor Antagonist into a 3-Selective High Affinity Fluorescent Probes Using Peptide-Based Linkers. *Organic & Biomolecular Chemistry*, **11**, 5673-5682. http://dx.doi.org/10.1039/c3ob41221k

[13] Smit, A.B., Syed, N.I., Schaap, D., van Minnen, J., Klumperman, J., Kits, K.S., Lodder, H., van der Schors, R.C., van Elk, R., Sorgedrager, B., Brejc, K., Sixma, T.K. and Geraerts, W.P. (2001) A Glia-Derived Acetylcholine-Binding Protein That Modulates Synaptic Transmission. *Nature*, **411**, 261-268. http://dx.doi.org/10.1038/35077000

[14] Hansen, S.B., Talley, T.T., Radić, Z. and Taylor, P. (2004) Structural and Ligand Recognition Characteristics of an Acetylcholine-Binding Protein from *Aplysia californica*. *Journal of Biological Chemistry*, **279**, 24197-24202. http://dx.doi.org/10.1074/jbc.M402452200

[15] McCormack, T., Petrovich, R.M., Mercier, K.A., DeRose, E.F., Cuneo, M.J., Williams, J., Johnson, K.L., Lamb, P.W., London, R.E. and Yakel, J.L. (2010) Identification and Functional Characterization of a Novel Acetylcholine-Binding

Protein from the Marine Annelid *Capitella teleta*. *Biochemistry*, **49**, 2279-2287. http://dx.doi.org/10.1021/bi902023y

[16] Rucktooa, P., Smit, A.B. and Sixma, T.K. (2009) Insight in Nachr Subtype Selectivity from Achbp Crystal Structures. *Biochemical Pharmacology*, **78**, 777-787. http://dx.doi.org/10.1016/j.bcp.2009.06.098

[17] Haddadian, E.J., Cheng, M.H., Coalson, R.D., Xu, Y. and Tang, P. (2008) In Silico Models for the Human Alpha4beta2 Nicotinic Acetylcholine Receptor. *Journal of Physical Chemistry B*, **112**, 13981-13990. http://dx.doi.org/10.1021/jp804868s

[18] Bisson, W.H., Westera, G., Schubiger, P.A. and Scapozza, L. (2008) Homology Modeling and Dynamics of the Extracellular Domain of Rat and Human Neuronal Nicotinic Acetylcholine Receptor Subtypes Alpha4beta2 and Alpha7. *Journal of Molecular Modeling*, **14**, 891-899. http://dx.doi.org/10.1007/s00894-008-0340-x

[19] Billen, B., Spurny, R., Brams, M., Van Elk, R., Valera-Kummer, S., Yakel, J.L., Voets, T., Bertrand, D., Smit, A.B. and Ulens, C. (2012) Molecular Actions of Smoking Cessation Drugs at *A4β2* Nicotinic Receptors Defined in Crystal Structures of a Homologous Binding Protein. *Proceedings of the National Academy of Sciences*, **109**, 9173-9178. http://dx.doi.org/10.1073/pnas.1116397109

[20] Ng, H.W., Laughton, C.A. and Doughty, S.W. (2013) Molecular Dynamics Simulations of the Adenosine A2a Receptor: Structural Stability, Sampling, and Convergence. *Journal of Chemical Information and Modeling*, **53**, 1168-1178. http://dx.doi.org/10.1021/ci300610w

[21] Ng, H.W., Laughton, C.A. and Doughty, S.W. (2014) Molecular Dynamics Simulations of the Adenosine A2a Receptor in Popc and Pope Lipid Bilayers: Effects of Membrane on Protein Behavior. *Journal of Chemical Information and Modeling*, **54**, 573-581. http://dx.doi.org/10.1021/ci400463z

[22] Marti-Renom, M.A., Stuart, A.C., Fiser, A., Sanchez, R., Melo, F. and Sali, A. (2000) Comparative Protein Structure Modeling of Genes and Genomes. *Annual Review of Biophysics and Biomolecular Structure*, **29**, 291-325. http://dx.doi.org/10.1146/annurev.biophys.29.1.291

[23] Hong, H., Hong, Q., Perkins, R., Shi, L., Fang, H., Su, Z., Dragan, Y., Fuscoe, J.C. and Tong, W. (2009) The Accurate Prediction of Protein Family from Amino Acid Sequence by Measuring Features of Sequence Fragments. *Journal of Computational Biology*, **16**, 1671-1688. http://dx.doi.org/10.1089/cmb.2008.0115

[24] Shen, J., Zhang, W., Fang, H., Perkins, R., Tong, W. and Hong, H. (2013) Homology Modeling, Molecular Docking, and Molecular Dynamics Simulations Elucidated Alpha-Fetoprotein Binding Modes. *BMC Bioinformatics*, **14**, S6. http://dx.doi.org/10.1186/1471-2105-14-S14-S6

[25] Maestro, S. (2011) Version 9.2. LLC, New York.

[26] Uniprot Consortium (2013) Update on Activities at the Universal Protein Resource (Uniprot) in 2013. *Nucleic Acids Research*, **41**, D43-D47. http://dx.doi.org/10.1093/nar/gks1068

[27] Hong, H., Neamati, N., Wang, S., Nicklaus, M.C., Mazumder, A., Zhao, H., Burke, T.R., Pommier, Y. and Milne, G.W.A. (1997) Discovery of Hiv-1 Integrase Inhibitors by Pharmacophore Searching. *Journal of Medicinal Chemistry*, **40**, 930-936. http://dx.doi.org/10.1021/jm960754h

[28] Neamati, N., Hong, H., Owen, J.M., Sunder, S., Winslow, H.E., Christensen, J.L., Zhao, H., Burke, T.R., Jr., Milne, G.W. and Pommier, Y. (1998) Salicylhydrazine-Containing Inhibitors of Hiv-1 Integrase: Implication for a Selective Chelation in the Integrase Active Site. *Journal of Medicinal Chemistry*, **41**, 3202-3209. http://dx.doi.org/10.1021/jm9801760

[29] Hong, H., Neamati, N., Winslow, H.E., Christensen, J.L., Orr, A., Pommier, Y. and Milne, G.W. (1998) Identification of Hiv-1 Integrase Inhibitors Based on a Four-Point Pharmacophore. *Antiviral Chemistry & Chemotherapy*, **9**, 461-472. http://dx.doi.org/10.1177/095632029800900602

[30] Hong, H., Fang, H., Xie, Q., Perkins, R., Sheehan, D.M. and Tong, W. (2003) Comparative Molecular Field Analysis (Comfa) Model Using a Large Diverse Set of Natural, Synthetic and Environmental Chemicals for Binding to the Androgen Receptor. *SAR and QSAR in Environmental Research*, **14**, 373-388. http://dx.doi.org/10.1080/10629360310001623962

[31] Shi, L., Tong, W., Fang, H., Xie, Q., Hong, H., Perkins, R., Wu, J., Tu, M., Blair, R.M., Branham, W.S., Waller, C., Walker, J. and Sheehan, D.M. (2002) An Integrated "4-Phase" Approach for Setting Endocrine Disruption Screening Priorities—Phase I and Ii Predictions of Estrogen Receptor Binding Affinity. *SAR and QSAR in Environmental Research*, **13**, 69-88. http://dx.doi.org/10.1080/10629360290002235

[32] Liu, J., Mansouri, K., Judson, R., Martin, M.T., Hong, H., Chen, M., Xu, X., Thomas, R. and Shah, I. (2015) Predicting Hepatotoxicity Using ToxCast *in Vitro* Bioactivity and Chemical Structure. *Chemical Research in Toxicology*, **28**, 738-751http://dx.doi.org/10.1021/tx500501h

[33] Hong, H., Tong, W., Fang, H., Shi, L., Xie, Q., Wu, J., Perkins, R., Walker, J.D., Branham, W. and Sheehan, D.M. (2002) Prediction of Estrogen Receptor Binding for 58,000 Chemicals Using an Integrated System of a Tree-Based Model with Structural Alerts. *Environmental Health Perspectives*, **110**, 29-36. http://dx.doi.org/10.1289/ehp.0211029

[34] Hong, H., Tong, W., Perkins, R., Fang, H., Xie, Q. and Shi, L. (2004) Multiclass Decision Forest-a Novel Pattern Recognition Method for Multiclass Classification in Microarray Data Analysis. *DNA and Cell Biology*, **23**, 685-694. http://dx.doi.org/10.1089/dna.2004.23.685

[35] Hong, H., Tong, W., Xie, Q., Fang, H. and Perkins, R. (2005) An in Silico Ensemble Method for Lead Discovery: Decision Forest. *SAR and QSAR in Environmental Research*, **16**, 339-347. http://dx.doi.org/10.1080/10659360500203022

[36] Tong, W., Hong, H., Fang, H., Xie, Q. and Perkins, R. (2003) Decision Forest: Combining the Predictions of Multiple Independent Decision Tree Models. *Journal of Chemical Information and Computer Science*, **43**, 525-531. http://dx.doi.org/10.1021/ci020058s

[37] Tong, W., Xie, Q., Hong, H., Shi, L., Fang, H., Perkins, R. and Petricoin, E.F. (2004) Using Decision Forest to Classify Prostate Cancer Samples on the Basis of Seldi-Tof Ms Data: Assessing Chance Correlation and Prediction Confidence. *Environmental Health Perspectives*, **112**, 1622-1627. http://dx.doi.org/10.1289/ehp.7109

[38] Xie, Q., Ratnasinghe, L.D., Hong, H., Perkins, R., Tang, Z.Z., Hu, N., Taylor, P.R. and Tong, W. (2005) Decision Forest Analysis of 61 Single Nucleotide Polymorphisms in a Case-Control Study of Esophageal Cancer; a Novel Method. *BMC Bioinformatics*, **6**, S4. http://dx.doi.org/10.1186/1471-2105-6-S2-S4

[39] Ng, H.W., Doughty, S.W., Luo, H., Ye, H., Ge, W., Tong, W. and Hong, H. (2015) Development and Validation of Decision Forest Model for Estrogen Receptor Binding Prediction of Chemicals Using Large Data Sets. *Chemical Research in Toxicology*, **28**, 2343-2351. http://dx.doi.org/10.1021/acs.chemrestox.5b00358

[40] McPhail, B., Tie, Y., Hong, H., Pearce, B.A., Schnackenberg, L.K., Ge, W., Valerio, L.G., Fuscoe, J.C., Tong, W., Buzatu, D.A., *et al.* (2012) Modeling Chemical Interaction Profiles: I. Spectral Data-Activity Relationship and Structure-Activity Relationship Models for Inhibitors and Non-Inhibitors of Cytochrome P450 CYP3A4 and CYP2D6 Isozymes. *Molecules*, **17**, 3283-3406. http://dx.doi.org/10.3390/molecules17033383

[41] Tong, W., Hong, H., Xie, Q., Shi, L., Fang, H. and Perkins, R. (2005) Assessing QSAR limitations—A Regulatory Perspective. *Current Computer-Aided Drug Design*, **1**, 195-205. http://dx.doi.org/10.2174/1573409053585663

[42] Hong, H., Xie, Q., Ge, W., Qian, F., Fang, H., Shi, L., Su, Z., Perkins, R. and Tong, W. (2008) Mold(2), Molecular Descriptors from 2d Structures for Chemoinformatics and Toxicoinformatics. *Journal of Chemical Information and Modeling*, **48**, 1337-1344. http://dx.doi.org/10.1021/ci800038f

[43] Hong, H. and Xin, X. (1990) ESSESA: An Expert System for Structure Elucidation from Spectra Analysis. 1. The Knowledge Base of Infrared Spectra and Analysis and Interpretation Program. *Journal of Chemical Information and Modeling*, **30**, 203-210. http://dx.doi.org/10.1021/ci00067a001

[44] Hong, H. and Xin, X. (1992) ESSESA: An Expert System for Structure Elucidation from Spectra Analysis. 2. A Novel Algorithm of Perception of the Linear Independent Smallest Set of Smallest Rings. *Analytica Chimica Acta*, **262**, 179-191. http://dx.doi.org/10.1016/0003-2670(92)80022-Y

[45] Hong, H. and Xin, X. (1992) ESSESA: An Expert System for Structure Elucidation from Spectra Analysis. 3. LNSCS for Chemical Knowledge Representation. *Journal of Chemical Information and Modeling*, **32**, 116-120. http://dx.doi.org/10.1021/ci00005a019

[46] Hong, H. and Xin, X. (1994) ESSESA: An Expert System for Structure Elucidation from Spectra Analysis. 4. Canonical Representation of Structures. *Journal of Chemical Information and Modeling*, **34**, 730-734. http://dx.doi.org/10.1021/ci00020a006

[47] Hong, H. and Xin, X. (1994) ESSESA: An Expert System for Structure Elucidation from Spectra Analysis. 5. Substructure Constraints from Analysis of First-Order 1H-NMR Spectra. *Journal of Chemical Information and Modeling*, **34**, 1259-1266. http://dx.doi.org/10.1021/ci00022a006

[48] Hong, H., Han, Y., Xin, X. and Shi, Y. (1995) ESSESA: An Expert System for Structure Elucidation from Spectra Analysis. 6. Substructure Constraints from Analysis of First-Order 13C-NMR Spectra. *Journal of Chemical Information and Modeling*, **35**, 979-1000. http://dx.doi.org/10.1021/ci00028a005

[49] Masui, H. and Hong, H. (2006) Spec2D: A Structure Elucidation System Based on 1H NMR and H-H COSY Spectra in Organic Chemistry. *Journal of Chemical Information and Modeling*, **46**, 775-787. http://dx.doi.org/10.1021/ci0502810

[50] Drake, R.R., Neamati, N., Hong, H., Pilon, A., Sunthankar, P., Hume, S.D., Wilne, G.W.A. and Pommier, Y. (1998) Identification of a Mononucleotide Binding Site in Human HIV-1 Integrase. *Proceedings of the National Academy of Sciences USA*, **98**, 1495-1500.

[51] Tie, Y., McPhail, B., Hong, H., Pearce, B.A., Schnackenberg, L.K., Ge, W., Buzatu, D.A., Wilkes, J.G., Fuscoe, J.C., Tong, W., *et al.* (2012) Modeling Chemical Interaction Profiles: II. Molecular Docking, Spectral Data-Activity Relationship, and Structure-Activity Relationship Models for Potent and Weak Inhibitors of Cytochrome p450 cyp3A4 Isozyme. *Molecules*, **17**, 3407-3460. http://dx.doi.org/10.3390/molecules17033407

[52] Ng, H.W., Perkins, R., Tong, W. and Hong, H. (2014) Versatility or Promiscuity: The Estrogen Receptors, Control of

Ligand Selectivity and an Update on Subtype Selective Ligands. *International Journal of Environmental Research and Public Health*, **11**, 8709-8742. http://dx.doi.org/10.3390/ijerph110908709

[53] Ng, H.W., Shu, M., Luo, H., Ye, H., Ge, W., Perkins, R., Tong, W. and Hong, H. (2015) Estrogenic Activity Data Extraction and in Silico Prediction Show the Endocrine Disruption Potential of Bisphenol a Replacement Compounds. *Chemical Research in Toxicology*, **28**, 1784-1795. http://dx.doi.org/10.1021/acs.chemrestox.5b00243

[54] Shen, J., Xu, L., Fang, H., Richard, A.M., Bray, J.D., Judson, R.S., Zhou, G., Colatsky, T.J., Aungst, J.L., Teng, C., Harris, S.C., Ge, W., Dai, S.Y., Su, Z., Jacobs, A.C., Harrouk, W., Perkins, R., Tong, W. and Hong, H. (2013) EADB: An Estrogenic Activity Database for Assessing Potential Endocrine Activity. *Toxicological Sciences*, **135**, 277-291. http://dx.doi.org/10.1093/toxsci/kft164

[55] Ding, D., Xu, L., Fang, H., Hong, H., Perkins, R., Harris, S., Bearden, E.D., Shi, L. and Tong, W. (2010) The Edkb: An Established Knowledge Base for Endocrine Disrupting Chemicals. *BMC Bioinformatics*, **11**, S5. http://dx.doi.org/10.1186/1471-2105-11-S6-S5

[56] Amber (2010) Version 11 University of California, San Francisco**.**

[57] Lindorff-Larsen, K., Piana, S., Palmo, K., Maragakis, P., Klepeis, J.L., Dror, R.O. and Shaw, D.E. (2010) Improved Side-Chain Torsion Potentials for the Amber Ff99sb Protein Force Field. *Proteins*: *Structure*, *Function, and Bioinformatics*, **78**, 1950-1958. http://dx.doi.org/10.1002/prot.22711

[58] Wang, J., Wolf, R.M., Caldwell, J.W., Kollman, P.A. and Case, D.A. (2004) Development and Testing of a General Amber Force Field. *Journal of Computational Chemistry*, **25**, 1157-1174. http://dx.doi.org/10.1002/jcc.20035

[59] Jakalian, A., Jack, D.B. and Bayly, C.I. (2002) Fast, Efficient Generation of High-Quality Atomic Charges. Am1-Bcc Model: Ii. Parameterization and Validation. *Journal of Computational Chemistry*, **23**, 1623-1641. http://dx.doi.org/10.1002/jcc.10128

[60] Ryckaert, J.-P., Ciccotti, G. and Berendsen, H.J. (1977) Numerical Integration of the Cartesian Equations of Motion of a System with Constraints: Molecular Dynamics of n-Alkanes. *Journal of Computational Physics*, **23**, 327-341. http://dx.doi.org/10.1016/0021-9991(77)90098-5

[61] Darden, T., York, D. and Pedersen, L. (1993) Particle Mesh Ewald: An N·Log (N) Method for Ewald Sums in Large Systems. *The Journal of Chemical Physics*, **98**, 10089-10092. http://dx.doi.org/10.1063/1.464397

[62] Rost, B. (1999) Twilight Zone of Protein Sequence Alignments. *Protein Engineering*, **12**, 85-94. http://dx.doi.org/10.1093/protein/12.2.85

[63] Yang, A.-S. and Honig, B. (2000) An Integrated Approach to the Analysis and Modeling of Protein Sequences and Structures. Iii. A Comparative Study of Sequence Conservation in Protein Structural Families Using Multiple Structural Alignments. *Journal of Molecular Biology*, **301**, 691-711. http://dx.doi.org/10.1006/jmbi.2000.3975

[64] Raval, A., Piana, S., Eastwood, M.P., Dror, R.O. and Shaw, D.E. (2012) Refinement of Protein Structure Homology Models Via Long, All-Atom Molecular Dynamics Simulations. *Proteins*: *Structure*, *Function, and Bioinformatics*, **80**, 2071-2079. http://dx.doi.org/10.1002/prot.24098

[65] Cheng, X., Wang, H., Grant, B., Sine, S.M. and McCammon, J.A. (2006) Targeted Molecular Dynamics Study of C-Loop Closure and Channel Gating in Nicotinic Receptors. *PLoS Computational Biology*, **2**, e134. http://dx.doi.org/10.1371/journal.pcbi.0020134

[66] Liu, X., Xu, Y., Li, H., Wang, X., Jiang, H. and Barrantes, F.J. (2008) Mechanics of Channel Gating of the Nicotinic Acetylcholine Receptor. *PLoS Computational Biology*, **4**, e19. http://dx.doi.org/10.1371/journal.pcbi.0040019

[67] Cheng, M.H., Xu, Y. and Tang, P. (2009) Anionic Lipid and Cholesterol Interactions with *A4β2* Nachr: Insights from Md Simulations. *The Journal of Physical Chemistry B*, **113**, 6964-6970. http://dx.doi.org/10.1021/jp900714b

[68] Liu, L.T., Haddadian, E.J., Willenbring, D., Xu, Y. and Tang, P. (2009) Higher Susceptibility to Halothane Modulation in Open-Than in Closed-Channel *A4β2* Nachr Revealed by Molecular Dynamics Simulations. *The Journal of Physical Chemistry B*, **114**, 626-632. http://dx.doi.org/10.1021/jp908944e

[69] Shu, M., Lin, Z., Zhang, Y., Wu, Y., Mei, H. and Jiang, Y. (2011) Molecular Dynamics Simulation of Oseltamivir Resistance in Neuraminidase of Avian Influenza H5n1 Virus. *Journal of Molecular Modeling*, **17**, 587-592. http://dx.doi.org/10.1007/s00894-010-0757-x

[70] Halgren, T. (2007) New Method for Fast and Accurate Binding-Site Identification and Analysis. *Chemical Biology & Drug Design*, **69**, 146-8. http://dx.doi.org/10.1111/j.1747-0285.2007.00483.x

[71] Sousa, S.F., Fernandes, P.A. and Ramos, M.J. (2006) Protein-Ligand Docking: Current Status and Future Challenges. *Proteins*, **65**, 15-26. http://dx.doi.org/10.1002/prot.21082

[72] Cheng, T., Li, Q., Zhou, Z., Wang, Y. and Bryant, S.H. (2012) Structure-Based Virtual Screening for Drug Discovery: A Problem-Centric Review. *AAPS Journal*, **14**, 133-141. http://dx.doi.org/10.1208/s12248-012-9322-0

[73] Celie, P.H., van Rossum-Fikkert, S.E., van Dijk, W.J., Brejc, K., Smit, A.B. and Sixma, T.K. (2004) Nicotine and

Carbamylcholine Binding to Nicotinic Acetylcholine Receptors as Studied in Achbp Crystal Structures. *Neuron*, **41**, 907-914. http://dx.doi.org/10.1016/S0896-6273(04)00115-1

[74] Ihara, M., Okajima, T., Yamashita, A., Oda, T., Hirata, K., Nishiwaki, H., Morimoto, T., Akamatsu, M., Ashikawa, Y. and Kuroda, S.I. (2008) Crystal Structures of Lymnaea Stagnalis Achbp in Complex with Neonicotinoid Insecticides Imidacloprid and Clothianidin. *Invertebrate Neuroscience*, **8**, 71-81. http://dx.doi.org/10.1007/s10158-008-0069-3

[75] Rohde, L.A.H., Ahring, P.K., Jensen, M.L., Nielsen, E.O., Peters, D., Helgstrand, C., Krintel, C., Harpsoe, K., Gajhede, M., Kastrup, J.S. and Balle, T. (2012) Intersubunit Bridge Formation Governs Agonist Efficacy at Nicotinic Acetylcholine Alpha 4 Beta 2 Receptors Unique Role of Halogen Bonding Revealed. *Journal of Biological Chemistry*, **287**, 4248-4259. http://dx.doi.org/10.1074/jbc.M111.292243

[76] Rucktooa, P., Haseler, C.A., van Elk, R., Smit, A.B., Gallagher, T. and Sixma, T.K. (2012) Structural Characterization of Binding Mode of Smoking Cessation Drugs to Nicotinic Acetylcholine Receptors through Study of Ligand Complexes with Acetylcholine-Binding Protein. *Journal of Biological Chemistry*, **287**, 23283-23293. http://dx.doi.org/10.1074/jbc.M112.360347

[77] Xiu, X., Puskar, N.L., Shanata, J.A., Lester, H.A. and Dougherty, D.A. (2009) Nicotine Binding to Brain Receptors Requires a Strong Cation-π Interaction. *Nature*, **458**, 534-537. http://dx.doi.org/10.1038/nature07768

Supplementary Material

Table S1. Information on the 11 ligands used in this study.

ID	Compound	PDB ID	pKi
NCT	L-(-)-nicotine	1UW6	8.34
IM4	Imidacloprid	2ZJU	9.21
09O	1-(pyridin-3-yl)-1,4-diazepane	3U8J	9.14
09P	1-(5-ethoxypyridin-3-yl)-1,4-diazepane	3U8K	9.21
09Q	1-(5-phenylpyridin-3-yl)-1,4-diazepane	3U8L	9.10
09R	1-(6-bromopyridin-3-yl)-1,4-diazepane	3U8M	9.49
09S	1-(6-bromo-5-ethoxypyridin-3-yl)-1,4-diazepane	3U8N	9.60
L0B	Alpha-lobeline	4AFH	8.15
QMR	Varenicline	4AFT	10.30
SW4	2-[(1R,2S)-2-[5-[[(2S)-azetidin-2-yl]methoxy]pyridin- 3-yl]cyclopropyl]ethanol	4B5D	10.00
C5E	Cytisine	4BQT	9.77

Table S2. Results of search a4 subunit on the PDB. ID consists of PDB ID (the first 4 letters) and the subunit (the last letter).

ID	Score	Expect	Identity	Positives	Gaps	Resolution
2WN9_A	87.8	1.20E−20	28%	43%	2%	1.75
2WN9_B	87.8	1.20E−20	28%	43%	2%	1.75
2WN9_C	87.8	1.20E−20	28%	43%	2%	1.75
2WN9_D	87.8	1.20E−20	28%	43%	2%	1.75
2WN9_E	87.8	1.20E−20	28%	43%	2%	1.75
2PGZ_A	87.8	1.10E−20	28%	43%	2%	1.76
2PGZ_B	87.8	1.10E−20	28%	43%	2%	1.76
2PGZ_C	87.8	1.10E−20	28%	43%	2%	1.76
2PGZ_D	87.8	1.10E−20	28%	43%	2%	1.76
2PGZ_E	87.8	1.10E−20	28%	43%	2%	1.76
2WNJ_A	87.8	1.20E−20	28%	43%	2%	1.8
2WNJ_B	87.8	1.20E−20	28%	43%	2%	1.8
2WNJ_C	87.8	1.20E−20	28%	43%	2%	1.8
2WNJ_D	87.8	1.20E−20	28%	43%	2%	1.8
2WNJ_E	87.8	1.20E−20	28%	43%	2%	1.8
4AFH_A	99.8	6.30E−25	31%	48%	7%	1.88
4AFH_B	99.8	6.30E−25	31%	48%	7%	1.88
4AFH_C	99.8	6.30E−25	31%	48%	7%	1.88
4AFH_D	99.8	6.30E−25	31%	48%	7%	1.88
4AFH_E	99.8	6.30E−25	31%	48%	7%	1.88
2Y7Y_A	89.4	3.00E−21	29%	43%	2%	1.9

Continued

2Y7Y_B	89.4	3.00E−21	29%	43%	2%	1.9
2Y7Y_C	89.4	3.00E−21	29%	43%	2%	1.9
2Y7Y_D	89.4	3.00E−21	29%	43%	2%	1.9
2Y7Y_E	89.4	3.00E−21	29%	43%	2%	1.9
2XYS_A	89.4	3.00E−21	29%	43%	2%	1.909
2XYS_B	89.4	3.00E−21	29%	43%	2%	1.909
2XYS_C	89.4	3.00E−21	29%	43%	2%	1.909
2XYS_D	89.4	3.00E−21	29%	43%	2%	1.909
2XYS_E	89.4	3.00E−21	29%	43%	2%	1.909
3C84_A	87.8	1.00E−20	28%	43%	2%	1.94
3C84_B	87.8	1.00E−20	28%	43%	2%	1.94
3C84_C	87.8	1.00E−20	28%	43%	2%	1.94
3C84_D	87.8	1.00E−20	28%	43%	2%	1.94
3C84_E	87.8	1.00E−20	28%	43%	2%	1.94
2QC1_B	217.6	1.90E−70	52%	66%	0%	1.94
2YMD_A	90.1	1.30E−21	28%	42%	2%	1.96
2YMD_B	90.1	1.30E−21	28%	42%	2%	1.96
2YMD_C	90.1	1.30E−21	28%	42%	2%	1.96
2YMD_D	90.1	1.30E−21	28%	42%	2%	1.96
2YMD_E	90.1	1.30E−21	28%	42%	2%	1.96
2YMD_F	90.1	1.30E−21	28%	42%	2%	1.96
2YMD_G	90.1	1.30E−21	28%	42%	2%	1.96
2YMD_H	90.1	1.30E−21	28%	42%	2%	1.96
2YMD_I	90.1	1.30E−21	28%	42%	2%	1.96
2YMD_J	90.1	1.30E−21	28%	42%	2%	1.96
2BJ0_A	60.5	2.50E−11	22%	43%	3%	2
2BJ0_B	60.5	2.50E−11	22%	43%	3%	2
2BJ0_C	60.5	2.50E−11	22%	43%	3%	2
2BJ0_D	60.5	2.50E−11	22%	43%	3%	2
2BJ0_E	60.5	2.50E−11	22%	43%	3%	2
1A05_A	30.4	1.2	26%	43%	21%	2
1A05_B	30.4	1.2	26%	43%	21%	2
4AFG_A	99.8	6.30E−25	31%	48%	7%	2
4AFG_B	99.8	6.30E−25	31%	48%	7%	2
4AFG_C	99.8	6.30E−25	31%	48%	7%	2
4AFG_D	99.8	6.30E−25	31%	48%	7%	2
4AFG_E	99.8	6.30E−25	31%	48%	7%	2

Continued

2BYN_A	87.8	1.00E−20	28%	43%	2%	2.02
2BYN_B	87.8	1.00E−20	28%	43%	2%	2.02
2BYN_C	87.8	1.00E−20	28%	43%	2%	2.02
2BYN_D	87.8	1.00E−20	28%	43%	2%	2.02
2BYN_E	87.8	1.00E−20	28%	43%	2%	2.02
2BYS_A	87.8	1.00E−20	28%	43%	2%	2.05
2BYS_B	87.8	1.00E−20	28%	43%	2%	2.05
2BYS_C	87.8	1.00E−20	28%	43%	2%	2.05
2BYS_D	87.8	1.00E−20	28%	43%	2%	2.05
2BYS_E	87.8	1.00E−20	28%	43%	2%	2.05
2BYS_F	87.8	1.00E−20	28%	43%	2%	2.05
2BYS_G	87.8	1.00E−20	28%	43%	2%	2.05
2BYS_H	87.8	1.00E−20	28%	43%	2%	2.05
2BYS_I	87.8	1.00E−20	28%	43%	2%	2.05
2BYS_J	87.8	1.00E−20	28%	43%	2%	2.05
2XYT_A	89.4	3.00E−21	29%	43%	2%	2.05
2XYT_B	89.4	3.00E−21	29%	43%	2%	2.05
2XYT_C	89.4	3.00E−21	29%	43%	2%	2.05
2XYT_D	89.4	3.00E−21	29%	43%	2%	2.05
2XYT_E	89.4	3.00E−21	29%	43%	2%	2.05
2XYT_F	89.4	3.00E−21	29%	43%	2%	2.05
2XYT_G	89.4	3.00E−21	29%	43%	2%	2.05
2XYT_H	89.4	3.00E−21	29%	43%	2%	2.05
2XYT_I	89.4	3.00E−21	29%	43%	2%	2.05
2XYT_J	89.4	3.00E−21	29%	43%	2%	2.05
2BYP_A	88.2	6.80E−21	28%	43%	2%	2.07
2BYP_B	88.2	6.80E−21	28%	43%	2%	2.07
2BYP_C	88.2	6.80E−21	28%	43%	2%	2.07
2BYP_D	88.2	6.80E−21	28%	43%	2%	2.07
2BYP_E	88.2	6.80E−21	28%	43%	2%	2.07
3PEO_A	87.8	1.20E−20	28%	43%	2%	2.1
3PEO_B	87.8	1.20E−20	28%	43%	2%	2.1
3PEO_C	87.8	1.20E−20	28%	43%	2%	2.1
3PEO_D	87.8	1.20E−20	28%	43%	2%	2.1
3PEO_E	87.8	1.20E−20	28%	43%	2%	2.1
3PEO_F	87.8	1.20E−20	28%	43%	2%	2.1
3PEO_G	87.8	1.20E−20	28%	43%	2%	2.1

Continued

3PEO_H	87.8	1.20E−20	28%	43%	2%	2.1
3PEO_I	87.8	1.20E−20	28%	43%	2%	2.1
3PEO_J	87.8	1.20E−20	28%	43%	2%	2.1
1UW6_A	63.5	2.20E−12	26%	41%	7%	2.2
1UW6_B	63.5	2.20E−12	26%	41%	7%	2.2
1UW6_C	63.5	2.20E−12	26%	41%	7%	2.2
1UW6_D	63.5	2.20E−12	26%	41%	7%	2.2
1UW6_E	63.5	2.20E−12	26%	41%	7%	2.2
1UW6_F	63.5	2.20E−12	26%	41%	7%	2.2
1UW6_G	63.5	2.20E−12	26%	41%	7%	2.2
1UW6_H	63.5	2.20E−12	26%	41%	7%	2.2
1UW6_I	63.5	2.20E−12	26%	41%	7%	2.2
1UW6_J	63.5	2.20E−12	26%	41%	7%	2.2
1UW6_K	63.5	2.20E−12	26%	41%	7%	2.2
1UW6_L	63.5	2.20E−12	26%	41%	7%	2.2
1UW6_M	63.5	2.20E−12	26%	41%	7%	2.2
1UW6_N	63.5	2.20E−12	26%	41%	7%	2.2
1UW6_O	63.5	2.20E−12	26%	41%	7%	2.2
1UW6_P	63.5	2.20E−12	26%	41%	7%	2.2
1UW6_Q	63.5	2.20E−12	26%	41%	7%	2.2
1UX2_A	63.5	2.40E−12	26%	41%	7%	2.2
1UX2_B	63.5	2.40E−12	26%	41%	7%	2.2
1UX2_C	63.5	2.40E−12	26%	41%	7%	2.2
1UX2_D	63.5	2.40E−12	26%	41%	7%	2.2
1UX2_E	63.5	2.40E−12	26%	41%	7%	2.2
1UX2_F	63.5	2.40E−12	26%	41%	7%	2.2
1UX2_G	63.5	2.40E−12	26%	41%	7%	2.2
1UX2_H	63.5	2.40E−12	26%	41%	7%	2.2
1UX2_I	63.5	2.40E−12	26%	41%	7%	2.2
1UX2_J	63.5	2.40E−12	26%	41%	7%	2.2
2WNC_A	87.8	1.00E−20	28%	43%	2%	2.2
2WNC_B	87.8	1.00E−20	28%	43%	2%	2.2
2WNC_C	87.8	1.00E−20	28%	43%	2%	2.2
2WNC_D	87.8	1.00E−20	28%	43%	2%	2.2
2WNC_E	87.8	1.00E−20	28%	43%	2%	2.2
4B5D_A	99.8	6.30E−25	31%	48%	7%	2.2

Continued

4B5D_B	99.8	6.30E−25	31%	48%	7%	2.2
4B5D_C	99.8	6.30E−25	31%	48%	7%	2.2
4B5D_D	99.8	6.30E−25	31%	48%	7%	2.2
4B5D_E	99.8	6.30E−25	31%	48%	7%	2.2
2C9T_A	89.4	3.00E−21	29%	43%	2%	2.25
2C9T_B	89.4	3.00E−21	29%	43%	2%	2.25
2C9T_C	89.4	3.00E−21	29%	43%	2%	2.25
2C9T_D	89.4	3.00E−21	29%	43%	2%	2.25
2C9T_E	89.4	3.00E−21	29%	43%	2%	2.25
2C9T_F	89.4	3.00E−21	29%	43%	2%	2.25
2C9T_G	89.4	3.00E−21	29%	43%	2%	2.25
2C9T_H	89.4	3.00E−21	29%	43%	2%	2.25
2C9T_I	89.4	3.00E−21	29%	43%	2%	2.25
2C9T_J	89.4	3.00E−21	29%	43%	2%	2.25
3IGQ_A	31.6	0.3	25%	45%	9%	2.3
3IGQ_B	31.6	0.3	25%	45%	9%	2.3
3IGQ_C	31.6	0.3	25%	45%	9%	2.3
3IGQ_D	31.6	0.3	25%	45%	9%	2.3
3IGQ_E	31.6	0.3	25%	45%	9%	2.3
3IGQ_F	31.6	0.3	25%	45%	9%	2.3
4ALX_A	63.5	2.80E−12	25%	41%	7%	2.3
4ALX_B	63.5	2.80E−12	25%	41%	7%	2.3
4ALX_C	63.5	2.80E−12	25%	41%	7%	2.3
4ALX_D	63.5	2.80E−12	25%	41%	7%	2.3
4ALX_E	63.5	2.80E−12	25%	41%	7%	2.3
4ALX_F	63.5	2.80E−12	25%	41%	7%	2.3
4ALX_G	63.5	2.80E−12	25%	41%	7%	2.3
4ALX_H	63.5	2.80E−12	25%	41%	7%	2.3
4ALX_I	63.5	2.80E−12	25%	41%	7%	2.3
4ALX_J	63.5	2.80E−12	25%	41%	7%	2.3
4DBM_A	87.8	1.10E−20	28%	43%	2%	2.3
4DBM_B	87.8	1.10E−20	28%	43%	2%	2.3
4DBM_C	87.8	1.10E−20	28%	43%	2%	2.3
4DBM_D	87.8	1.10E−20	28%	43%	2%	2.3
4DBM_E	87.8	1.10E−20	28%	43%	2%	2.3
3U8L_A	63.5	2.00E−12	26%	41%	7%	2.32
3U8L_B	63.5	2.00E−12	26%	41%	7%	2.32

Continued

3U8L_C	63.5	2.00E−12	26%	41%	7%	2.32
3U8L_D	63.5	2.00E−12	26%	41%	7%	2.32
3U8L_E	63.5	2.00E−12	26%	41%	7%	2.32
3U8L_F	63.5	2.00E−12	26%	41%	7%	2.32
3U8L_G	63.5	2.00E−12	26%	41%	7%	2.32
3U8L_H	63.5	2.00E−12	26%	41%	7%	2.32
3U8L_I	63.5	2.00E−12	26%	41%	7%	2.32
3U8L_J	63.5	2.00E−12	26%	41%	7%	2.32
3SIO_A	85.9	4.80E−20	28%	42%	2%	2.32
3SIO_B	85.9	4.80E−20	28%	42%	2%	2.32
3SIO_C	85.9	4.80E−20	28%	42%	2%	2.32
3SIO_D	85.9	4.80E−20	28%	42%	2%	2.32
3SIO_E	85.9	4.80E−20	28%	42%	2%	2.32
3SIO_F	85.9	4.80E−20	28%	42%	2%	2.32
3SIO_G	85.9	4.80E−20	28%	42%	2%	2.32
3SIO_H	85.9	4.80E−20	28%	42%	2%	2.32
3SIO_I	85.9	4.80E−20	28%	42%	2%	2.32
3SIO_J	85.9	4.80E−20	28%	42%	2%	2.32
3U8J_A	63.5	2.00E−12	26%	41%	7%	2.35
3U8J_B	63.5	2.00E−12	26%	41%	7%	2.35
3U8J_C	63.5	2.00E−12	26%	41%	7%	2.35
3U8J_D	63.5	2.00E−12	26%	41%	7%	2.35
3U8J_E	63.5	2.00E−12	26%	41%	7%	2.35
3U8J_F	63.5	2.00E−12	26%	41%	7%	2.35
3U8J_G	63.5	2.00E−12	26%	41%	7%	2.35
3U8J_H	63.5	2.00E−12	26%	41%	7%	2.35
3U8J_I	63.5	2.00E−12	26%	41%	7%	2.35
3U8J_J	63.5	2.00E−12	26%	41%	7%	2.35
3U8N_A	63.5	2.00E−12	26%	41%	7%	2.35
3U8N_B	63.5	2.00E−12	26%	41%	7%	2.35
3U8N_C	63.5	2.00E−12	26%	41%	7%	2.35
3U8N_D	63.5	2.00E−12	26%	41%	7%	2.35
3U8N_E	63.5	2.00E−12	26%	41%	7%	2.35
3U8N_F	63.5	2.00E−12	26%	41%	7%	2.35
3U8N_G	63.5	2.00E−12	26%	41%	7%	2.35
3U8N_H	63.5	2.00E−12	26%	41%	7%	2.35
3U8N_I	63.5	2.00E−12	26%	41%	7%	2.35

Continued

3U8N_J	63.5	2.00E−12	26%	41%	7%	2.35
3U8N_K	63.5	2.00E−12	26%	41%	7%	2.35
3U8N_L	63.5	2.00E−12	26%	41%	7%	2.35
3U8N_M	63.5	2.00E−12	26%	41%	7%	2.35
3U8N_N	63.5	2.00E−12	26%	41%	7%	2.35
3U8N_O	63.5	2.00E−12	26%	41%	7%	2.35
3U8N_P	63.5	2.00E−12	26%	41%	7%	2.35
3U8N_Q	63.5	2.00E−12	26%	41%	7%	2.35
3U8N_R	63.5	2.00E−12	26%	41%	7%	2.35
3U8N_S	63.5	2.00E−12	26%	41%	7%	2.35
3U8N_T	63.5	2.00E−12	26%	41%	7%	2.35
2X00_A	87.8	1.20E−20	28%	43%	2%	2.4
2X00_B	87.8	1.20E−20	28%	43%	2%	2.4
2X00_C	87.8	1.20E−20	28%	43%	2%	2.4
2X00_D	87.8	9.60E−21	28%	43%	2%	2.4
2X00_E	87.8	1.20E−20	28%	43%	2%	2.4
2BR8_A	89.4	3.00E−21	29%	43%	2%	2.4
2BR8_B	89.4	3.00E−21	29%	43%	2%	2.4
2BR8_C	89.4	3.00E−21	29%	43%	2%	2.4
2BR8_D	89.4	3.00E−21	29%	43%	2%	2.4
2BR8_E	89.4	3.00E−21	29%	43%	2%	2.4
2UZ6_A	89.4	3.00E−21	29%	43%	2%	2.4
2UZ6_B	89.4	3.00E−21	29%	43%	2%	2.4
2UZ6_C	89.4	3.00E−21	29%	43%	2%	2.4
2UZ6_D	89.4	3.00E−21	29%	43%	2%	2.4
2UZ6_E	89.4	3.00E−21	29%	43%	2%	2.4
2UZ6_F	89.4	3.00E−21	29%	43%	2%	2.4
2UZ6_G	89.4	3.00E−21	29%	43%	2%	2.4
2UZ6_H	89.4	3.00E−21	29%	43%	2%	2.4
2UZ6_I	89.4	3.00E−21	29%	43%	2%	2.4
2UZ6_J	89.4	3.00E−21	29%	43%	2%	2.4
2YME_A	92.4	2.00E−22	29%	43%	2%	2.4
2YME_B	92.4	2.00E−22	29%	43%	2%	2.4
2YME_C	92.4	2.00E−22	29%	43%	2%	2.4
2YME_D	92.4	2.00E−22	29%	43%	2%	2.4
2YME_E	92.4	2.00E−22	29%	43%	2%	2.4
2YME_F	92.4	2.00E−22	29%	43%	2%	2.4

Continued

2YME_G	92.4	2.00E−22	29%	43%	2%	2.4
2YME_H	92.4	2.00E−22	29%	43%	2%	2.4
2YME_I	92.4	2.00E−22	29%	43%	2%	2.4
2YME_J	92.4	2.00E−22	29%	43%	2%	2.4
2XNV_A	90.9	9.90E−22	27%	44%	2%	2.44
2XNV_B	90.9	9.90E−22	27%	44%	2%	2.44
2XNV_C	90.9	9.90E−22	27%	44%	2%	2.44
2XNV_D	90.9	9.90E−22	27%	44%	2%	2.44
2XNV_E	90.9	9.90E−22	27%	44%	2%	2.44
2XNV_F	90.9	9.90E−22	27%	44%	2%	2.44
2XNV_G	90.9	9.90E−22	27%	44%	2%	2.44
2XNV_H	90.9	9.90E−22	27%	44%	2%	2.44
2XNV_I	90.9	9.90E−22	27%	44%	2%	2.44
2XNV_J	90.9	9.90E−22	27%	44%	2%	2.44
3PMZ_A	87.8	1.00E−20	28%	43%	2%	2.44
3PMZ_B	87.8	1.00E−20	28%	43%	2%	2.44
3PMZ_C	87.8	1.00E−20	28%	43%	2%	2.44
3PMZ_D	87.8	1.00E−20	28%	43%	2%	2.44
3PMZ_E	87.8	1.00E−20	28%	43%	2%	2.44
3PMZ_F	87.8	1.00E−20	28%	43%	2%	2.44
3PMZ_G	87.8	1.00E−20	28%	43%	2%	2.44
3PMZ_H	87.8	1.00E−20	28%	43%	2%	2.44
3PMZ_I	87.8	1.00E−20	28%	43%	2%	2.44
3PMZ_J	87.8	1.00E−20	28%	43%	2%	2.44
2BYR_A	87.8	1.00E−20	28%	43%	2%	2.45
2BYR_B	87.8	1.00E−20	28%	43%	2%	2.45
2BYR_C	87.8	1.00E−20	28%	43%	2%	2.45
2BYR_D	87.8	1.00E−20	28%	43%	2%	2.45
2BYR_E	87.8	1.00E−20	28%	43%	2%	2.45
2BYR_F	87.8	1.00E−20	28%	43%	2%	2.45
2BYR_G	87.8	1.00E−20	28%	43%	2%	2.45
2BYR_H	87.8	1.00E−20	28%	43%	2%	2.45
2BYR_I	87.8	1.00E−20	28%	43%	2%	2.45
2BYR_J	87.8	1.00E−20	28%	43%	2%	2.45
3U8K_A	63.5	2.00E−12	26%	41%	7%	2.47
3U8K_B	63.5	2.00E−12	26%	41%	7%	2.47
3U8K_C	63.5	2.00E−12	26%	41%	7%	2.47

Continued

3U8K_D	63.5	2.00E−12	26%	41%	7%	2.47
3U8K_E	63.5	2.00E−12	26%	41%	7%	2.47
3U8K_F	63.5	2.00E−12	26%	41%	7%	2.47
3U8K_G	63.5	2.00E−12	26%	41%	7%	2.47
3U8K_H	63.5	2.00E−12	26%	41%	7%	2.47
3U8K_I	63.5	2.00E−12	26%	41%	7%	2.47
3U8K_J	63.5	2.00E−12	26%	41%	7%	2.47
3U8K_K	63.5	2.00E−12	26%	41%	7%	2.47
3U8K_L	63.5	2.00E−12	26%	41%	7%	2.47
3U8K_M	63.5	2.00E−12	26%	41%	7%	2.47
3U8K_N	63.5	2.00E−12	26%	41%	7%	2.47
3U8K_O	63.5	2.00E−12	26%	41%	7%	2.47
3U8K_P	63.5	2.00E−12	26%	41%	7%	2.47
3U8K_Q	63.5	2.00E−12	26%	41%	7%	2.47
3U8K_R	63.5	2.00E−12	26%	41%	7%	2.47
3U8K_S	63.5	2.00E−12	26%	41%	7%	2.47
3U8K_T	63.5	2.00E−12	26%	41%	7%	2.47
3C79_A	87.8	1.00E−20	28%	43%	2%	2.48
3C79_B	87.8	1.00E−20	28%	43%	2%	2.48
3C79_C	87.8	1.00E−20	28%	43%	2%	2.48
3C79_D	87.8	1.00E−20	28%	43%	2%	2.48
3C79_E	87.8	1.00E−20	28%	43%	2%	2.48
1UV6_A	63.5	2.00E−12	26%	41%	7%	2.5
1UV6_B	63.5	2.00E−12	26%	41%	7%	2.5
1UV6_C	63.5	2.00E−12	26%	41%	7%	2.5
1UV6_D	63.5	2.00E−12	26%	41%	7%	2.5
1UV6_E	63.5	2.00E−12	26%	41%	7%	2.5
1UV6_F	63.5	2.00E−12	26%	41%	7%	2.5
1UV6_G	63.5	2.00E−12	26%	41%	7%	2.5
1UV6_H	63.5	2.00E−12	26%	41%	7%	2.5
1UV6_I	63.5	2.00E−12	26%	41%	7%	2.5
1UV6_J	63.5	2.00E−12	26%	41%	7%	2.5
3C75_L	27.7	5.3	27%	41%	11%	2.5
3C75_M	27.7	5.3	27%	41%	11%	2.5
2WZY_A	87.8	1.20E−20	28%	43%	2%	2.51
2WZY_B	87.8	1.20E−20	28%	43%	2%	2.51
2WZY_C	87.8	1.20E−20	28%	43%	2%	2.51

Continued

2WZY_D	87.8	1.20E−20	28%	43%	2%	2.51
2WZY_E	87.8	1.20E−20	28%	43%	2%	2.51
2WZY_F	87.8	1.20E−20	28%	43%	2%	2.51
2WZY_G	87.8	1.20E−20	28%	43%	2%	2.51
2WZY_H	87.8	1.20E−20	28%	43%	2%	2.51
2WZY_I	87.8	1.20E−20	28%	43%	2%	2.51
2WZY_J	87.8	1.20E−20	28%	43%	2%	2.51
2XNU_A	90.9	9.90E−22	27%	44%	2%	2.55
2XNU_B	90.9	9.90E−22	27%	44%	2%	2.55
2XNU_C	90.9	9.90E−22	27%	44%	2%	2.55
2XNU_D	90.9	9.90E−22	27%	44%	2%	2.55
2XNU_E	90.9	9.90E−22	27%	44%	2%	2.55
2ZJU_A	65.5	5.50E−13	26%	41%	7%	2.58
2ZJU_B	65.5	5.50E−13	26%	41%	7%	2.58
2ZJU_C	65.5	5.50E−13	26%	41%	7%	2.58
2ZJU_D	65.5	5.50E−13	26%	41%	7%	2.58
2ZJU_E	65.5	5.50E−13	26%	41%	7%	2.58
3TLW_A	33.1	0.12	24%	43%	13%	2.6
3TLW_B	33.1	0.12	24%	43%	13%	2.6
3TLW_C	33.1	0.12	24%	43%	13%	2.6
3TLW_D	33.1	0.12	24%	43%	13%	2.6
3TLW_E	33.1	0.12	24%	43%	13%	2.6
2W8G_A	89.4	3.00E−21	29%	43%	2%	2.6
2W8G_B	89.4	3.00E−21	29%	43%	2%	2.6
2W8G_C	89.4	3.00E−21	29%	43%	2%	2.6
2W8G_D	89.4	3.00E−21	29%	43%	2%	2.6
2W8G_E	89.4	3.00E−21	29%	43%	2%	2.6
1I9B_A	63.5	2.30E−12	26%	41%	7%	2.7
1I9B_B	63.5	2.30E−12	26%	41%	7%	2.7
1I9B_C	63.5	2.30E−12	26%	41%	7%	2.7
1I9B_D	63.5	2.30E−12	26%	41%	7%	2.7
1I9B_E	63.5	2.30E−12	26%	41%	7%	2.7
2ZJV_A	65.5	5.50E−13	26%	41%	7%	2.7
2ZJV_B	65.5	5.50E−13	26%	41%	7%	2.7
2ZJV_C	65.5	5.50E−13	26%	41%	7%	2.7
2ZJV_D	65.5	5.50E−13	26%	41%	7%	2.7
2ZJV_E	65.5	5.50E−13	26%	41%	7%	2.7

Continued

3U8M_A	63.5	2.00E−12	26%	41%	7%	2.7
3U8M_B	63.5	2.00E−12	26%	41%	7%	2.7
3U8M_C	63.5	2.00E−12	26%	41%	7%	2.7
3U8M_D	63.5	2.00E−12	26%	41%	7%	2.7
3U8M_E	63.5	2.00E−12	26%	41%	7%	2.7
3U8M_F	63.5	2.00E−12	26%	41%	7%	2.7
3U8M_G	63.5	2.00E−12	26%	41%	7%	2.7
3U8M_H	63.5	2.00E−12	26%	41%	7%	2.7
3U8M_I	63.5	2.00E−12	26%	41%	7%	2.7
3U8M_J	63.5	2.00E−12	26%	41%	7%	2.7
3U8M_K	63.5	2.00E−12	26%	41%	7%	2.7
3U8M_L	63.5	2.00E−12	26%	41%	7%	2.7
3U8M_M	63.5	2.00E−12	26%	41%	7%	2.7
3U8M_N	63.5	2.00E−12	26%	41%	7%	2.7
3U8M_O	63.5	2.00E−12	26%	41%	7%	2.7
3U8M_P	63.5	2.00E−12	26%	41%	7%	2.7
3U8M_Q	63.5	2.00E−12	26%	41%	7%	2.7
3U8M_R	63.5	2.00E−12	26%	41%	7%	2.7
3U8M_S	63.5	2.00E−12	26%	41%	7%	2.7
3U8M_T	63.5	2.00E−12	26%	41%	7%	2.7
2WNL_A	87.8	1.00E−20	28%	43%	2%	2.7
2WNL_B	87.8	1.00E−20	28%	43%	2%	2.7
2WNL_C	87.8	1.00E−20	28%	43%	2%	2.7
2WNL_D	87.8	1.00E−20	28%	43%	2%	2.7
2WNL_E	87.8	1.00E−20	28%	43%	2%	2.7
2WNL_F	87.8	1.00E−20	28%	43%	2%	2.7
2WNL_G	87.8	1.00E−20	28%	43%	2%	2.7
2WNL_H	87.8	1.00E−20	28%	43%	2%	2.7
2WNL_I	87.8	1.00E−20	28%	43%	2%	2.7
2WNL_J	87.8	1.00E−20	28%	43%	2%	2.7
2W8F_A	89.4	3.00E−21	29%	43%	2%	2.7
2W8F_B	89.4	3.00E−21	29%	43%	2%	2.7
2W8F_C	89.4	3.00E−21	29%	43%	2%	2.7
2W8F_D	89.4	3.00E−21	29%	43%	2%	2.7
2W8F_E	89.4	3.00E−21	29%	43%	2%	2.7
2W8F_F	89.4	3.00E−21	29%	43%	2%	2.7
2W8F_G	89.4	3.00E−21	29%	43%	2%	2.7

Continued

2W8F_H	89.4	3.00E−21	29%	43%	2%	2.7
2W8F_I	89.4	3.00E−21	29%	43%	2%	2.7
2W8F_J	89.4	3.00E−21	29%	43%	2%	2.7
2XZ5_A	87.8	1.10E−20	29%	43%	2%	2.8
2XZ5_B	87.8	1.10E−20	29%	43%	2%	2.8
2XZ5_C	87.8	1.10E−20	29%	43%	2%	2.8
2XZ5_D	87.8	1.10E−20	29%	43%	2%	2.8
2XZ5_E	87.8	1.10E−20	29%	43%	2%	2.8
3SQ6_A	104.4	6.40E−27	31%	48%	3%	2.8
3SQ6_B	104.4	6.40E−27	31%	48%	3%	2.8
3SQ6_C	104.4	6.40E−27	31%	48%	3%	2.8
3SQ6_D	104.4	6.40E−27	31%	48%	3%	2.8
3SQ6_E	104.4	6.40E−27	31%	48%	3%	2.8
3SQ6_F	104.4	6.40E−27	31%	48%	3%	2.8
3SQ6_G	104.4	6.40E−27	31%	48%	3%	2.8
3SQ6_H	104.4	6.40E−27	31%	48%	3%	2.8
3SQ6_I	104.4	6.40E−27	31%	48%	3%	2.8
3SQ6_J	104.4	6.40E−27	31%	48%	3%	2.8
1IQP_A	30.4	1.1	38%	48%	0%	2.8
1IQP_B	30.4	1.1	38%	48%	0%	2.8
1IQP_C	30.4	1.1	38%	48%	0%	2.8
1IQP_D	30.4	1.1	38%	48%	0%	2.8
1IQP_E	30.4	1.1	38%	48%	0%	2.8
1IQP_F	30.4	1.1	38%	48%	0%	2.8
3TLU_A	33.1	0.12	24%	43%	13%	2.85
3TLU_B	33.1	0.12	24%	43%	13%	2.85
3TLU_C	33.1	0.12	24%	43%	13%	2.85
3TLU_D	33.1	0.12	24%	43%	13%	2.85
3TLU_E	33.1	0.12	24%	43%	13%	2.85
2PH9_A	87.8	1.10E−20	28%	43%	2%	2.88
2PH9_B	87.8	1.10E−20	28%	43%	2%	2.88
2PH9_C	87.8	1.10E−20	28%	43%	2%	2.88
2PH9_D	87.8	1.10E−20	28%	43%	2%	2.88
2PH9_E	87.8	1.10E−20	28%	43%	2%	2.88
3TLV_A	33.5	0.11	24%	43%	13%	2.9
3TLV_B	33.5	0.11	24%	43%	13%	2.9
3TLV_C	33.5	0.11	24%	43%	13%	2.9

Continued

3TLV_D	33.5	0.11	24%	43%	13%	2.9
3TLV_E	33.5	0.11	24%	43%	13%	2.9
3UU5_A	33.5	0.12	24%	43%	13%	2.9
3UU5_B	33.5	0.12	24%	43%	13%	2.9
3UU5_C	33.5	0.12	24%	43%	13%	2.9
3UU5_D	33.5	0.12	24%	43%	13%	2.9
3UU5_E	33.5	0.12	24%	43%	13%	2.9
3UUB_A	33.1	0.12	24%	43%	13%	2.9
3UUB_B	33.1	0.12	24%	43%	13%	2.9
3UUB_C	33.1	0.12	24%	43%	13%	2.9
3UUB_D	33.1	0.12	24%	43%	13%	2.9
3UUB_E	33.1	0.12	24%	43%	13%	2.9
3UUB_F	33.1	0.12	24%	43%	13%	2.9
3UUB_G	33.1	0.12	24%	43%	13%	2.9
3UUB_H	33.1	0.12	24%	43%	13%	2.9
3UUB_I	33.1	0.12	24%	43%	13%	2.9
3UUB_J	33.1	0.12	24%	43%	13%	2.9
3EAM_A	36.6	0.0088	25%	44%	13%	2.9
3EAM_B	36.6	0.0088	25%	44%	13%	2.9
3EAM_C	36.6	0.0088	25%	44%	13%	2.9
3EAM_D	36.6	0.0088	25%	44%	13%	2.9
3EAM_E	36.6	0.0088	25%	44%	13%	2.9
3SH1_A	93.2	1.40E−22	30%	44%	2%	2.9
3SH1_B	93.2	1.40E−22	30%	44%	2%	2.9
3SH1_C	93.2	1.40E−22	30%	44%	2%	2.9
3SH1_D	93.2	1.40E−22	30%	44%	2%	2.9
3SH1_E	93.2	1.40E−22	30%	44%	2%	2.9
3SH1_F	93.2	1.40E−22	30%	44%	2%	2.9
3SH1_G	93.2	1.40E−22	30%	44%	2%	2.9
3SH1_H	93.2	1.40E−22	30%	44%	2%	2.9
3SH1_I	93.2	1.40E−22	30%	44%	2%	2.9
3SH1_J	93.2	1.40E−22	30%	44%	2%	2.9
3RQW_A	42.4	0.00013	22%	41%	5%	2.91
3RQW_B	42.4	0.00013	22%	41%	5%	2.91
3RQW_C	42.4	0.00013	22%	41%	5%	2.91
3RQW_D	42.4	0.00013	22%	41%	5%	2.91
3RQW_E	42.4	0.00013	22%	41%	5%	2.91

Continued

3RQW_F	42.4	0.00013	22%	41%	5%	2.91
3RQW_G	42.4	0.00013	22%	41%	5%	2.91
3RQW_H	42.4	0.00013	22%	41%	5%	2.91
3RQW_I	42.4	0.00013	22%	41%	5%	2.91
3RQW_J	42.4	0.00013	22%	41%	5%	2.91
3UU6_A	33.5	0.11	24%	43%	13%	2.98
3UU6_B	33.5	0.11	24%	43%	13%	2.98
3UU6_C	33.5	0.11	24%	43%	13%	2.98
3UU6_D	33.5	0.11	24%	43%	13%	2.98
3UU6_E	33.5	0.11	24%	43%	13%	2.98
4F8H_A	37.7	0.0046	24%	42%	11%	2.99
4F8H_B	37.7	0.0046	24%	42%	11%	2.99
4F8H_C	37.7	0.0046	24%	42%	11%	2.99
4F8H_D	37.7	0.0046	24%	42%	11%	2.99
4F8H_E	37.7	0.0046	24%	42%	11%	2.99
2BR7_A	89.4	3.00E−21	29%	43%	2%	3
2BR7_B	89.4	3.00E−21	29%	43%	2%	3
2BR7_C	89.4	3.00E−21	29%	43%	2%	3
2BR7_D	89.4	3.00E−21	29%	43%	2%	3
2BR7_E	89.4	3.00E−21	29%	43%	2%	3
3T4M_A	102.1	8.20E−26	31%	45%	2%	3
3T4M_B	102.1	8.20E−26	31%	45%	2%	3
3T4M_C	102.1	8.20E−26	31%	45%	2%	3
3T4M_D	102.1	8.20E−26	31%	45%	2%	3
3T4M_E	102.1	8.20E−26	31%	45%	2%	3
3T4M_F	102.1	8.20E−26	31%	45%	2%	3
3T4M_G	102.1	8.20E−26	31%	45%	2%	3
3T4M_H	102.1	8.20E−26	31%	45%	2%	3
3T4M_I	102.1	8.20E−26	31%	45%	2%	3
3T4M_J	102.1	8.20E−26	31%	45%	2%	3
3UU4_A	33.1	0.12	24%	43%	13%	3.05
3UU4_B	33.1	0.12	24%	43%	13%	3.05
3UU4_C	33.1	0.12	24%	43%	13%	3.05
3UU4_D	33.1	0.12	24%	43%	13%	3.05
3UU4_E	33.1	0.12	24%	43%	13%	3.05
3RQU_A	42.4	0.00013	22%	41%	5%	3.09
3RQU_B	42.4	0.00013	22%	41%	5%	3.09

Continued

3RQU_C	42.4	0.00013	22%	41%	5%	3.09
3RQU_D	42.4	0.00013	22%	41%	5%	3.09
3RQU_E	42.4	0.00013	22%	41%	5%	3.09
3RQU_F	42.4	0.00013	22%	41%	5%	3.09
3RQU_G	42.4	0.00013	22%	41%	5%	3.09
3RQU_H	42.4	0.00013	22%	41%	5%	3.09
3RQU_I	42.4	0.00013	22%	41%	5%	3.09
3RQU_J	42.4	0.00013	22%	41%	5%	3.09
3EHZ_A	37.7	0.0046	24%	42%	11%	3.1
3EHZ_B	37.7	0.0046	24%	42%	11%	3.1
3EHZ_C	37.7	0.0046	24%	42%	11%	3.1
3EHZ_D	37.7	0.0046	24%	42%	11%	3.1
3EHZ_E	37.7	0.0046	24%	42%	11%	3.1
3GUA_A	87.8	9.10E−21	28%	43%	2%	3.1
3GUA_B	87.8	9.10E−21	28%	43%	2%	3.1
3GUA_C	87.8	9.10E−21	28%	43%	2%	3.1
3GUA_D	87.8	9.10E−21	28%	43%	2%	3.1
3GUA_E	87.8	9.10E−21	28%	43%	2%	3.1
3GUA_F	87.8	9.10E−21	28%	43%	2%	3.1
3GUA_G	87.8	9.10E−21	28%	43%	2%	3.1
3GUA_H	87.8	9.10E−21	28%	43%	2%	3.1
3GUA_I	87.8	9.10E−21	28%	43%	2%	3.1
3GUA_J	87.8	9.10E−21	28%	43%	2%	3.1
3SQ9_A	104.4	6.40E−27	31%	48%	3%	3.1
3SQ9_B	104.4	6.40E−27	31%	48%	3%	3.1
3SQ9_C	104.4	6.40E−27	31%	48%	3%	3.1
3SQ9_D	104.4	6.40E−27	31%	48%	3%	3.1
3SQ9_E	104.4	6.40E−27	31%	48%	3%	3.1
3SQ9_F	104.4	6.40E−27	31%	48%	3%	3.1
3SQ9_G	104.4	6.40E−27	31%	48%	3%	3.1
3SQ9_H	104.4	6.40E−27	31%	48%	3%	3.1
3SQ9_I	104.4	6.40E−27	31%	48%	3%	3.1
3SQ9_J	104.4	6.40E−27	31%	48%	3%	3.1
2XZ6_A	87.8	9.30E−21	29%	43%	2%	3.137
2XZ6_B	87.8	9.30E−21	29%	43%	2%	3.137
2XZ6_C	87.8	9.30E−21	29%	43%	2%	3.137
2XZ6_D	87.8	9.30E−21	29%	43%	2%	3.137

Continued

2XZ6_E	87.8	9.30E−21	29%	43%	2%	3.137
2XZ6_F	87.8	9.30E−21	29%	43%	2%	3.137
2XZ6_G	87.8	9.30E−21	29%	43%	2%	3.137
2XZ6_H	87.8	9.30E−21	29%	43%	2%	3.137
2XZ6_I	87.8	9.30E−21	29%	43%	2%	3.137
2XZ6_J	87.8	9.30E−21	29%	43%	2%	3.137
3UU3_A	33.5	0.12	24%	43%	13%	3.15
3UU3_B	33.5	0.12	24%	43%	13%	3.15
3UU3_C	33.5	0.12	24%	43%	13%	3.15
3UU3_D	33.5	0.12	24%	43%	13%	3.15
3UU3_E	33.5	0.12	24%	43%	13%	3.15
3LSV_A	36.6	0.0093	25%	44%	13%	3.15
3LSV_B	36.6	0.0093	25%	44%	13%	3.15
3LSV_C	36.6	0.0093	25%	44%	13%	3.15
3LSV_D	36.6	0.0093	25%	44%	13%	3.15
3LSV_E	36.6	0.0093	25%	44%	13%	3.15
2XQ9_A	37.7	0.0045	24%	42%	11%	3.2
2XQ9_B	37.7	0.0045	24%	42%	11%	3.2
2XQ9_C	37.7	0.0045	24%	42%	11%	3.2
2XQ9_D	37.7	0.0045	24%	42%	11%	3.2
2XQ9_E	37.7	0.0045	24%	42%	11%	3.2
3P4W_A	36.6	0.0089	25%	44%	13%	3.2
3P4W_B	36.6	0.0089	25%	44%	13%	3.2
3P4W_C	36.6	0.0089	25%	44%	13%	3.2
3P4W_D	36.6	0.0089	25%	44%	13%	3.2
3P4W_E	36.6	0.0089	25%	44%	13%	3.2
3TLS_A	36.6	0.0094	25%	44%	13%	3.2
3TLS_B	36.6	0.0094	25%	44%	13%	3.2
3TLS_C	36.6	0.0094	25%	44%	13%	3.2
3TLS_D	36.6	0.0094	25%	44%	13%	3.2
3TLS_E	36.6	0.0094	25%	44%	13%	3.2
4AFT_A	89.4	3.00E−21	29%	43%	2%	3.2
4AFT_B	89.4	3.00E−21	29%	43%	2%	3.2
4AFT_C	89.4	3.00E−21	29%	43%	2%	3.2
4AFT_D	89.4	3.00E−21	29%	43%	2%	3.2
4AFT_E	89.4	3.00E−21	29%	43%	2%	3.2
2XNT_A	90.9	9.90E−22	27%	44%	2%	3.21

Continued

2XNT_B	90.9	9.90E−22	27%	44%	2%	3.21
2XNT_C	90.9	9.90E−22	27%	44%	2%	3.21
2XNT_D	90.9	9.90E−22	27%	44%	2%	3.21
2XNT_E	90.9	9.90E−22	27%	44%	2%	3.21
2XNT_F	90.9	9.90E−22	27%	44%	2%	3.21
2XNT_G	90.9	9.90E−22	27%	44%	2%	3.21
2XNT_H	90.9	9.90E−22	27%	44%	2%	3.21
2XNT_I	90.9	9.90E−22	27%	44%	2%	3.21
2XNT_J	90.9	9.90E−22	27%	44%	2%	3.21
3UU8_A	33.1	0.12	24%	43%	13%	3.25
3UU8_B	33.1	0.12	24%	43%	13%	3.25
3UU8_C	33.1	0.12	24%	43%	13%	3.25
3UU8_D	33.1	0.12	24%	43%	13%	3.25
3UU8_E	33.1	0.12	24%	43%	13%	3.25
2Y58_A	89.4	3.00E−21	29%	43%	2%	3.25
2Y58_B	89.4	3.00E−21	29%	43%	2%	3.25
2Y58_C	89.4	3.00E−21	29%	43%	2%	3.25
2Y58_D	89.4	3.00E−21	29%	43%	2%	3.25
2Y58_E	89.4	3.00E−21	29%	43%	2%	3.25
3RHW_A	45.1	1.70E−05	23%	42%	8%	3.26
3RHW_B	45.1	1.70E−05	23%	42%	8%	3.26
3RHW_C	45.1	1.70E−05	23%	42%	8%	3.26
3RHW_D	45.1	1.70E−05	23%	42%	8%	3.26
3RHW_E	45.1	1.70E−05	23%	42%	8%	3.26
2VL0_A	43.9	3.60E−05	22%	41%	4%	3.3
2VL0_B	43.9	3.60E−05	22%	41%	4%	3.3
2VL0_C	43.9	3.60E−05	22%	41%	4%	3.3
2VL0_D	43.9	3.60E−05	22%	41%	4%	3.3
2VL0_E	43.9	3.60E−05	22%	41%	4%	3.3
2VL0_F	43.9	3.60E−05	22%	41%	4%	3.3
2VL0_G	43.9	3.60E−05	22%	41%	4%	3.3
2VL0_H	43.9	3.60E−05	22%	41%	4%	3.3
2VL0_I	43.9	3.60E−05	22%	41%	4%	3.3
2VL0_J	43.9	3.60E−05	22%	41%	4%	3.3
2YKS_A	43.9	3.60E−05	22%	41%	4%	3.3
2YKS_B	43.9	3.60E−05	22%	41%	4%	3.3
2YKS_C	43.9	3.60E−05	22%	41%	4%	3.3

Continued

2YKS_D	43.9	3.60E−05	22%	41%	4%	3.3
2YKS_E	43.9	3.60E−05	22%	41%	4%	3.3
2YKS_F	43.9	3.60E−05	22%	41%	4%	3.3
2YKS_G	43.9	3.60E−05	22%	41%	4%	3.3
2YKS_H	43.9	3.60E−05	22%	41%	4%	3.3
2YKS_I	43.9	3.60E−05	22%	41%	4%	3.3
2YKS_J	43.9	3.60E−05	22%	41%	4%	3.3
3P50_A	36.6	0.0089	25%	44%	13%	3.3
3P50_B	36.6	0.0089	25%	44%	13%	3.3
3P50_C	36.6	0.0089	25%	44%	13%	3.3
3P50_D	36.6	0.0089	25%	44%	13%	3.3
3P50_E	36.6	0.0089	25%	44%	13%	3.3
3TLT_A	37	0.0083	25%	44%	13%	3.3
3TLT_B	37	0.0083	25%	44%	13%	3.3
3TLT_C	37	0.0083	25%	44%	13%	3.3
3TLT_D	37	0.0083	25%	44%	13%	3.3
3TLT_E	37	0.0083	25%	44%	13%	3.3
2Y57_A	89.4	3.00E−21	29%	43%	2%	3.3
2Y57_B	89.4	3.00E−21	29%	43%	2%	3.3
2Y57_C	89.4	3.00E−21	29%	43%	2%	3.3
2Y57_D	89.4	3.00E−21	29%	43%	2%	3.3
2Y57_E	89.4	3.00E−21	29%	43%	2%	3.3
2YN6_A	42.4	0.00013	22%	41%	5%	3.31
2YN6_B	42.4	0.00013	22%	41%	5%	3.31
2YN6_C	42.4	0.00013	22%	41%	5%	3.31
2YN6_D	42.4	0.00013	22%	41%	5%	3.31
2YN6_E	42.4	0.00013	22%	41%	5%	3.31
4A97_A	41.2	0.00027	21%	41%	4%	3.34
4A97_B	41.2	0.00027	21%	41%	4%	3.34
4A97_C	41.2	0.00027	21%	41%	4%	3.34
4A97_D	41.2	0.00027	21%	41%	4%	3.34
4A97_E	41.2	0.00027	21%	41%	4%	3.34
4A97_F	41.2	0.00027	21%	41%	4%	3.34
4A97_G	41.2	0.00027	21%	41%	4%	3.34
4A97_H	41.2	0.00027	21%	41%	4%	3.34
4A97_I	41.2	0.00027	21%	41%	4%	3.34
4A97_J	41.2	0.00027	21%	41%	4%	3.34

Continued

3RIF_A	45.1	1.70E−05	23%	42%	8%	3.35
3RIF_B	45.1	1.70E−05	23%	42%	8%	3.35
3RIF_C	45.1	1.70E−05	23%	42%	8%	3.35
3RIF_D	45.1	1.70E−05	23%	42%	8%	3.35
3RIF_E	45.1	1.70E−05	23%	42%	8%	3.35
3RI5_A	45.1	1.70E−05	23%	42%	8%	3.4
3RI5_B	45.1	1.70E−05	23%	42%	8%	3.4
3RI5_C	45.1	1.70E−05	23%	42%	8%	3.4
3RI5_D	45.1	1.70E−05	23%	42%	8%	3.4
3RI5_E	45.1	1.70E−05	23%	42%	8%	3.4
2XQ7_A	37.7	0.0046	24%	42%	11%	3.4
2XQ7_B	37.7	0.0046	24%	42%	11%	3.4
2XQ7_C	37.7	0.0046	24%	42%	11%	3.4
2XQ7_D	37.7	0.0046	24%	42%	11%	3.4
2XQ7_E	37.7	0.0046	24%	42%	11%	3.4
2BYQ_A	87.8	1.00E−20	28%	43%	2%	3.4
2BYQ_B	87.8	1.00E−20	28%	43%	2%	3.4
2BYQ_C	87.8	1.00E−20	28%	43%	2%	3.4
2BYQ_D	87.8	1.00E−20	28%	43%	2%	3.4
2BYQ_E	87.8	1.00E−20	28%	43%	2%	3.4
3UQ4_A	43.1	6.30E−05	22%	41%	5%	3.5
3UQ4_B	43.1	6.30E−05	22%	41%	5%	3.5
3UQ4_C	43.1	6.30E−05	22%	41%	5%	3.5
3UQ4_D	43.1	6.30E−05	22%	41%	5%	3.5
3UQ4_E	43.1	6.30E−05	22%	41%	5%	3.5
3UQ4_F	43.1	6.30E−05	22%	41%	5%	3.5
3UQ4_G	43.1	6.30E−05	22%	41%	5%	3.5
3UQ4_H	43.1	6.30E−05	22%	41%	5%	3.5
3UQ4_I	43.1	6.30E−05	22%	41%	5%	3.5
3UQ4_J	43.1	6.30E−05	22%	41%	5%	3.5
2XQ3_A	37.7	0.0046	24%	42%	11%	3.5
2XQ3_B	37.7	0.0046	24%	42%	11%	3.5
2XQ3_C	37.7	0.0046	24%	42%	11%	3.5
2XQ3_D	37.7	0.0046	24%	42%	11%	3.5
2XQ3_E	37.7	0.0046	24%	42%	11%	3.5
2XQ5_A	37.7	0.0046	24%	42%	11%	3.5
2XQ5_B	37.7	0.0046	24%	42%	11%	3.5
2XQ5_C	37.7	0.0046	24%	42%	11%	3.5
2XQ5_D	37.7	0.0046	24%	42%	11%	3.5
2XQ5_E	37.7	0.0046	24%	42%	11%	3.5

Continued

3EI0_A	37.7	0.0048	24%	42%	11%	3.5
3EI0_B	37.7	0.0048	24%	42%	11%	3.5
3EI0_C	37.7	0.0048	24%	42%	11%	3.5
3EI0_D	37.7	0.0048	24%	42%	11%	3.5
3EI0_E	37.7	0.0048	24%	42%	11%	3.5
2Y56_A	89.4	3.00E−21	29%	43%	2%	3.59
2Y56_B	89.4	3.00E−21	29%	43%	2%	3.59
2Y56_C	89.4	3.00E−21	29%	43%	2%	3.59
2Y56_D	89.4	3.00E−21	29%	43%	2%	3.59
2Y56_E	89.4	3.00E−21	29%	43%	2%	3.59
2XQ4_A	37.7	0.0046	24%	42%	11%	3.6
2XQ4_B	37.7	0.0046	24%	42%	11%	3.6
2XQ4_C	37.7	0.0046	24%	42%	11%	3.6
2XQ4_D	37.7	0.0046	24%	42%	11%	3.6
2XQ4_E	37.7	0.0046	24%	42%	11%	3.6
2XQ8_A	37.7	0.0046	24%	42%	11%	3.6
2XQ8_B	37.7	0.0046	24%	42%	11%	3.6
2XQ8_C	37.7	0.0046	24%	42%	11%	3.6
2XQ8_D	37.7	0.0046	24%	42%	11%	3.6
2XQ8_E	37.7	0.0046	24%	42%	11%	3.6
4A98_A	41.2	0.00027	21%	41%	4%	3.61
4A98_B	41.2	0.00027	21%	41%	4%	3.61
4A98_C	41.2	0.00027	21%	41%	4%	3.61
4A98_D	41.2	0.00027	21%	41%	4%	3.61
4A98_E	41.2	0.00027	21%	41%	4%	3.61
4A98_F	41.2	0.00027	21%	41%	4%	3.61
4A98_G	41.2	0.00027	21%	41%	4%	3.61
4A98_H	41.2	0.00027	21%	41%	4%	3.61
4A98_I	41.2	0.00027	21%	41%	4%	3.61
4A98_J	41.2	0.00027	21%	41%	4%	3.61
3ZKR_A	41.2	0.00027	21%	41%	4%	3.65
3ZKR_B	41.2	0.00027	21%	41%	4%	3.65
3ZKR_C	41.2	0.00027	21%	41%	4%	3.65
3ZKR_D	41.2	0.00027	21%	41%	4%	3.65
3ZKR_E	41.2	0.00027	21%	41%	4%	3.65
3ZKR_F	41.2	0.00027	21%	41%	4%	3.65
3ZKR_G	41.2	0.00027	21%	41%	4%	3.65
3ZKR_H	41.2	0.00027	21%	41%	4%	3.65
3ZKR_I	41.2	0.00027	21%	41%	4%	3.65
3ZKR_J	41.2	0.00027	21%	41%	4%	3.65

Continued

2Y54_A	89.4	3.00E−21	29%	43%	2%	3.65
2Y54_B	89.4	3.00E−21	29%	43%	2%	3.65
2Y54_C	89.4	3.00E−21	29%	43%	2%	3.65
2Y54_D	89.4	3.00E−21	29%	43%	2%	3.65
2Y54_E	89.4	3.00E−21	29%	43%	2%	3.65
2XQ6_A	37.7	0.0046	24%	42%	11%	3.7
2XQ6_B	37.7	0.0046	24%	42%	11%	3.7
2XQ6_C	37.7	0.0046	24%	42%	11%	3.7
2XQ6_D	37.7	0.0046	24%	42%	11%	3.7
2XQ6_E	37.7	0.0046	24%	42%	11%	3.7
2XQA_A	37.7	0.0046	24%	42%	11%	3.7
2XQA_B	37.7	0.0046	24%	42%	11%	3.7
2XQA_C	37.7	0.0046	24%	42%	11%	3.7
2XQA_D	37.7	0.0046	24%	42%	11%	3.7
2XQA_E	37.7	0.0046	24%	42%	11%	3.7
3UQ7_A	43.1	6.50E−05	22%	41%	5%	3.8
3UQ7_B	43.1	6.50E−05	22%	41%	5%	3.8
3UQ7_C	43.1	6.50E−05	22%	41%	5%	3.8
3UQ7_D	43.1	6.50E−05	22%	41%	5%	3.8
3UQ7_E	43.1	6.50E−05	22%	41%	5%	3.8
3UQ7_F	43.1	6.50E−05	22%	41%	5%	3.8
3UQ7_G	43.1	6.50E−05	22%	41%	5%	3.8
3UQ7_H	43.1	6.50E−05	22%	41%	5%	3.8
3UQ7_I	43.1	6.50E−05	22%	41%	5%	3.8
3UQ7_J	43.1	6.50E−05	22%	41%	5%	3.8
3RIA_A	45.1	1.70E−05	23%	42%	8%	3.8
3RIA_B	45.1	1.70E−05	23%	42%	8%	3.8
3RIA_C	45.1	1.70E−05	23%	42%	8%	3.8
3RIA_D	45.1	1.70E−05	23%	42%	8%	3.8
3RIA_E	45.1	1.70E−05	23%	42%	8%	3.8
4AR2_A	34.7	0.056	25%	47%	16%	3.8
2YOE_A	41.2	0.00027	21%	41%	4%	3.9
2YOE_B	41.2	0.00027	21%	41%	4%	3.9
2YOE_C	41.2	0.00027	21%	41%	4%	3.9
2YOE_D	41.2	0.00027	21%	41%	4%	3.9
2YOE_E	41.2	0.00027	21%	41%	4%	3.9
2YOE_F	41.2	0.00027	21%	41%	4%	3.9
2YOE_G	41.2	0.00027	21%	41%	4%	3.9
2YOE_H	41.2	0.00027	21%	41%	4%	3.9
2YOE_I	41.2	0.00027	21%	41%	4%	3.9

Continued

2YOE_J	41.2	0.00027	21%	41%	4%	3.9
2BG9_C	158.3	9.40E−46	38%	59%	3%	4
2BG9_B	176.8	1.10E−52	43%	62%	1%	4
2BG9_E	174.5	8.60E−52	43%	67%	0%	4
2BG9_A	222.6	2.60E−70	51%	67%	0%	4
2BG9_D	222.6	2.60E−70	51%	67%	0%	4
3UQ5_A	43.1	6.20E−05	22%	41%	5%	4.2
3UQ5_B	43.1	6.20E−05	22%	41%	5%	4.2
3UQ5_C	43.1	6.20E−05	22%	41%	5%	4.2
3UQ5_D	43.1	6.20E−05	22%	41%	5%	4.2
3UQ5_E	43.1	6.20E−05	22%	41%	5%	4.2
3UQ5_F	43.1	6.20E−05	22%	41%	5%	4.2
3UQ5_G	43.1	6.20E−05	22%	41%	5%	4.2
3UQ5_H	43.1	6.20E−05	22%	41%	5%	4.2
3UQ5_I	43.1	6.20E−05	22%	41%	5%	4.2
3UQ5_J	43.1	6.20E−05	22%	41%	5%	4.2
1YI5_A	63.5	2.00E−12	26%	41%	7%	4.2
1YI5_B	63.5	2.00E−12	26%	41%	7%	4.2
1YI5_C	63.5	2.00E−12	26%	41%	7%	4.2
1YI5_D	63.5	2.00E−12	26%	41%	7%	4.2
1YI5_E	63.5	2.00E−12	26%	41%	7%	4.2
4AQQ_A	34.7	0.056	25%	47%	16%	4.75
4AOE_A	73.9	5.40E−16	24%	44%	3%	5.8
4AOE_B	73.9	5.40E−16	24%	44%	3%	5.8
4AOE_C	73.9	5.40E−16	24%	44%	3%	5.8
4AOE_D	73.9	5.40E−16	24%	44%	3%	5.8
4AOE_E	73.9	5.40E−16	24%	44%	3%	5.8
4AOD_A	75.1	2.10E−16	24%	46%	3%	6
4AOD_B	75.1	2.10E−16	24%	46%	3%	6
4AOD_C	75.1	2.10E−16	24%	46%	3%	6
4AOD_D	75.1	2.10E−16	24%	46%	3%	6
4AOD_E	75.1	2.10E−16	24%	46%	3%	6
4AQ5_C	156.4	5.40E−44	36%	57%	7%	6.2
4AQ9_C	156.4	5.40E−44	36%	57%	7%	6.2
4AQ5_B	171	1.60E−49	41%	58%	6%	6.2
4AQ9_B	171	1.60E−49	41%	58%	6%	6.2
4AQ5_E	168.7	9.40E−49	42%	64%	4%	6.2
4AQ9_E	168.7	9.40E−49	42%	64%	4%	6.2
4AQ5_A	222.2	2.80E−69	51%	67%	0%	6.2
4AQ5_D	222.2	2.80E−69	51%	67%	0%	6.2
4AQ9_A	222.2	2.80E−69	51%	67%	0%	6.2
4AQ9_D	222.2	2.80E−69	51%	67%	0%	6.2

Table S3. Results of search b2 subunit on the PDB. ID consists of PDB ID (the first 4 letters) and the subunit (the last letter).

ID	Score	Expect	Identity	Positives	Gaps	Resolution
2R31_A	28.1	4.5	53%	69%	0%	1
2RB8_A	26.6	7.6	27%	39%	19%	1.45
2WN9_A	63.5	2.20E−12	24%	44%	4%	1.75
2WN9_B	63.5	2.20E−12	24%	44%	4%	1.75
2WN9_C	63.5	2.20E−12	24%	44%	4%	1.75
2WN9_D	63.5	2.20E−12	24%	44%	4%	1.75
2WN9_E	63.5	2.20E−12	24%	44%	4%	1.75
2PGZ_A	63.5	2.30E−12	24%	44%	4%	1.76
2PGZ_B	63.5	2.30E−12	24%	44%	4%	1.76
2PGZ_C	63.5	2.30E−12	24%	44%	4%	1.76
2PGZ_D	63.5	2.30E−12	24%	44%	4%	1.76
2PGZ_E	63.5	2.30E−12	24%	44%	4%	1.76
2WNJ_A	63.5	2.20E−12	24%	44%	4%	1.8
2WNJ_B	63.5	2.20E−12	24%	44%	4%	1.8
2WNJ_C	63.5	2.20E−12	24%	44%	4%	1.8
2WNJ_D	63.5	2.20E−12	24%	44%	4%	1.8
2WNJ_E	63.5	2.20E−12	24%	44%	4%	1.8
2ZD2_A	28.1	4.3	53%	69%	0%	1.8
2ZD2_B	28.1	4.3	53%	69%	0%	1.8
4AFH_A	70.1	1.30E−14	28%	46%	8%	1.88
4AFH_B	70.1	1.30E−14	28%	46%	8%	1.88
4AFH_C	70.1	1.30E−14	28%	46%	8%	1.88
4AFH_D	70.1	1.30E−14	28%	46%	8%	1.88
4AFH_E	70.1	1.30E−14	28%	46%	8%	1.88
2Y7Y_A	63.9	1.50E−12	25%	45%	4%	1.9
2Y7Y_B	63.9	1.50E−12	25%	45%	4%	1.9
2Y7Y_C	63.9	1.50E−12	25%	45%	4%	1.9
2Y7Y_D	63.9	1.50E−12	25%	45%	4%	1.9
2Y7Y_E	63.9	1.50E−12	25%	45%	4%	1.9
2P4X_A	28.1	4.5	53%	69%	0%	1.9
2P4X_B	28.1	4.5	53%	69%	0%	1.9
2XYS_A	63.9	1.50E−12	25%	45%	4%	1.909
2XYS_B	63.9	1.50E−12	25%	45%	4%	1.909
2XYS_C	63.9	1.50E−12	25%	45%	4%	1.909
2XYS_D	63.9	1.50E−12	25%	45%	4%	1.909

Continued

2XYS_E	63.9	1.50E−12	25%	45%	4%	1.909
3C84_A	63.5	2.60E−12	24%	44%	4%	1.94
3C84_B	63.5	2.60E−12	24%	44%	4%	1.94
3C84_C	63.5	2.60E−12	24%	44%	4%	1.94
3C84_D	63.5	2.60E−12	24%	44%	4%	1.94
3C84_E	63.5	2.60E−12	24%	44%	4%	1.94
2QC1_B	176.4	2.10E−54	42%	63%	2%	1.94
1OSP_L	28.1	4.8	23%	42%	7%	1.95
2YMD_A	64.7	8.20E−13	25%	42%	1%	1.96
2YMD_B	64.7	8.20E−13	25%	42%	1%	1.96
2YMD_C	64.7	8.20E−13	25%	42%	1%	1.96
2YMD_D	64.7	8.20E−13	25%	42%	1%	1.96
2YMD_E	64.7	8.20E−13	25%	42%	1%	1.96
2YMD_F	64.7	8.20E−13	25%	42%	1%	1.96
2YMD_G	64.7	8.20E−13	25%	42%	1%	1.96
2YMD_H	64.7	8.20E−13	25%	42%	1%	1.96
2YMD_I	64.7	8.20E−13	25%	42%	1%	1.96
2YMD_J	64.7	8.20E−13	25%	42%	1%	1.96
2BJ0_A	51.6	4.10E−08	28%	48%	5%	2
2BJ0_B	51.6	4.10E−08	28%	48%	5%	2
2BJ0_C	51.6	4.10E−08	28%	48%	5%	2
2BJ0_D	51.6	4.10E−08	28%	48%	5%	2
2BJ0_E	51.6	4.10E−08	28%	48%	5%	2
4AFG_A	70.1	1.30E−14	28%	46%	8%	2
4AFG_B	70.1	1.30E−14	28%	46%	8%	2
4AFG_C	70.1	1.30E−14	28%	46%	8%	2
4AFG_D	70.1	1.30E−14	28%	46%	8%	2
4AFG_E	70.1	1.30E−14	28%	46%	8%	2
2BYN_A	63.5	2.60E−12	24%	44%	4%	2.02
2BYN_B	63.5	2.60E−12	24%	44%	4%	2.02
2BYN_C	63.5	2.60E−12	24%	44%	4%	2.02
2BYN_D	63.5	2.60E−12	24%	44%	4%	2.02
2BYN_E	63.5	2.60E−12	24%	44%	4%	2.02
2BYS_A	63.5	2.60E−12	24%	44%	4%	2.05
2BYS_B	63.5	2.60E−12	24%	44%	4%	2.05
2BYS_C	63.5	2.60E−12	24%	44%	4%	2.05
2BYS_D	63.5	2.60E−12	24%	44%	4%	2.05

Continued

2BYS_E	63.5	2.60E−12	24%	44%	4%	2.05
2BYS_F	63.5	2.60E−12	24%	44%	4%	2.05
2BYS_G	63.5	2.60E−12	24%	44%	4%	2.05
2BYS_H	63.5	2.60E−12	24%	44%	4%	2.05
2BYS_I	63.5	2.60E−12	24%	44%	4%	2.05
2BYS_J	63.5	2.60E−12	24%	44%	4%	2.05
2XYT_A	63.9	1.50E−12	25%	45%	4%	2.05
2XYT_B	63.9	1.50E−12	25%	45%	4%	2.05
2XYT_C	63.9	1.50E−12	25%	45%	4%	2.05
2XYT_D	63.9	1.50E−12	25%	45%	4%	2.05
2XYT_E	63.9	1.50E−12	25%	45%	4%	2.05
2XYT_F	63.9	1.50E−12	25%	45%	4%	2.05
2XYT_G	63.9	1.50E−12	25%	45%	4%	2.05
2XYT_H	63.9	1.50E−12	25%	45%	4%	2.05
2XYT_I	63.9	1.50E−12	25%	45%	4%	2.05
2XYT_J	63.9	1.50E−12	25%	45%	4%	2.05
2BYP_A	63.5	2.20E−12	24%	43%	1%	2.07
2BYP_B	63.5	2.20E−12	24%	43%	1%	2.07
2BYP_C	63.5	2.20E−12	24%	43%	1%	2.07
2BYP_D	63.5	2.20E−12	24%	43%	1%	2.07
2BYP_E	63.5	2.20E−12	24%	43%	1%	2.07
3PEO_A	63.5	2.20E−12	24%	44%	4%	2.1
3PEO_B	63.5	2.20E−12	24%	44%	4%	2.1
3PEO_C	63.5	2.20E−12	24%	44%	4%	2.1
3PEO_D	63.5	2.20E−12	24%	44%	4%	2.1
3PEO_E	63.5	2.20E−12	24%	44%	4%	2.1
3PEO_F	63.5	2.20E−12	24%	44%	4%	2.1
3PEO_G	63.5	2.20E−12	24%	44%	4%	2.1
3PEO_H	63.5	2.20E−12	24%	44%	4%	2.1
3PEO_I	63.5	2.20E−12	24%	44%	4%	2.1
3PEO_J	63.5	2.20E−12	24%	44%	4%	2.1
1UW6_A	44.3	2.20E−05	24%	40%	3%	2.2
1UW6_B	44.3	2.20E−05	24%	40%	3%	2.2
1UW6_C	44.3	2.20E−05	24%	40%	3%	2.2
1UW6_D	44.3	2.20E−05	24%	40%	3%	2.2
1UW6_E	44.3	2.20E−05	24%	40%	3%	2.2
1UW6_F	44.3	2.20E−05	24%	40%	3%	2.2

Continued

1UW6_G	44.3	2.20E−05	24%	40%	3%	2.2
1UW6_H	44.3	2.20E−05	24%	40%	3%	2.2
1UW6_I	44.3	2.20E−05	24%	40%	3%	2.2
1UW6_J	44.3	2.20E−05	24%	40%	3%	2.2
1UW6_K	44.3	2.20E−05	24%	40%	3%	2.2
1UW6_L	44.3	2.20E−05	24%	40%	3%	2.2
1UW6_M	44.3	2.20E−05	24%	40%	3%	2.2
1UW6_N	44.3	2.20E−05	24%	40%	3%	2.2
1UW6_O	44.3	2.20E−05	24%	40%	3%	2.2
1UW6_P	44.3	2.20E−05	24%	40%	3%	2.2
1UW6_Q	44.3	2.20E−05	24%	40%	3%	2.2
1UX2_A	43.9	2.40E−05	24%	40%	3%	2.2
1UX2_B	43.9	2.40E−05	24%	40%	3%	2.2
1UX2_C	43.9	2.40E−05	24%	40%	3%	2.2
1UX2_D	43.9	2.40E−05	24%	40%	3%	2.2
1UX2_E	43.9	2.40E−05	24%	40%	3%	2.2
1UX2_F	43.9	2.40E−05	24%	40%	3%	2.2
1UX2_G	43.9	2.40E−05	24%	40%	3%	2.2
1UX2_H	43.9	2.40E−05	24%	40%	3%	2.2
1UX2_I	43.9	2.40E−05	24%	40%	3%	2.2
1UX2_J	43.9	2.40E−05	24%	40%	3%	2.2
2WNC_A	63.5	2.60E−12	24%	44%	4%	2.2
2WNC_B	63.5	2.60E−12	24%	44%	4%	2.2
2WNC_C	63.5	2.60E−12	24%	44%	4%	2.2
2WNC_D	63.5	2.60E−12	24%	44%	4%	2.2
2WNC_E	63.5	2.60E−12	24%	44%	4%	2.2
4B5D_A	70.1	1.30E−14	28%	46%	8%	2.2
4B5D_B	70.1	1.30E−14	28%	46%	8%	2.2
4B5D_C	70.1	1.30E−14	28%	46%	8%	2.2
4B5D_D	70.1	1.30E−14	28%	46%	8%	2.2
4B5D_E	70.1	1.30E−14	28%	46%	8%	2.2
2C9T_A	63.9	1.50E−12	25%	45%	4%	2.25
2C9T_B	63.9	1.50E−12	25%	45%	4%	2.25
2C9T_C	63.9	1.50E−12	25%	45%	4%	2.25
2C9T_D	63.9	1.50E−12	25%	45%	4%	2.25
2C9T_E	63.9	1.50E−12	25%	45%	4%	2.25
2C9T_F	63.9	1.50E−12	25%	45%	4%	2.25

Continued

2C9T_G	63.9	1.50E−12	25%	45%	4%	2.25
2C9T_H	63.9	1.50E−12	25%	45%	4%	2.25
2C9T_I	63.9	1.50E−12	25%	45%	4%	2.25
2C9T_J	63.9	1.50E−12	25%	45%	4%	2.25
4ALX_A	43.9	3.40E−05	24%	40%	3%	2.3
4ALX_B	43.9	3.40E−05	24%	40%	3%	2.3
4ALX_C	43.9	3.40E−05	24%	40%	3%	2.3
4ALX_D	43.9	3.40E−05	24%	40%	3%	2.3
4ALX_E	43.9	3.40E−05	24%	40%	3%	2.3
4ALX_F	43.9	3.40E−05	24%	40%	3%	2.3
4ALX_G	43.9	3.40E−05	24%	40%	3%	2.3
4ALX_H	43.9	3.40E−05	24%	40%	3%	2.3
4ALX_I	43.9	3.40E−05	24%	40%	3%	2.3
4ALX_J	43.9	3.40E−05	24%	40%	3%	2.3
4DBM_A	63.5	2.30E−12	24%	44%	4%	2.3
4DBM_B	63.5	2.30E−12	24%	44%	4%	2.3
4DBM_C	63.5	2.30E−12	24%	44%	4%	2.3
4DBM_D	63.5	2.30E−12	24%	44%	4%	2.3
4DBM_E	63.5	2.30E−12	24%	44%	4%	2.3
3U8L_A	44.3	2.20E−05	24%	40%	3%	2.32
3U8L_B	44.3	2.20E−05	24%	40%	3%	2.32
3U8L_C	44.3	2.20E−05	24%	40%	3%	2.32
3U8L_D	44.3	2.20E−05	24%	40%	3%	2.32
3U8L_E	44.3	2.20E−05	24%	40%	3%	2.32
3U8L_F	44.3	2.20E−05	24%	40%	3%	2.32
3U8L_G	44.3	2.20E−05	24%	40%	3%	2.32
3U8L_H	44.3	2.20E−05	24%	40%	3%	2.32
3U8L_I	44.3	2.20E−05	24%	40%	3%	2.32
3U8L_J	44.3	2.20E−05	24%	40%	3%	2.32
3SIO_A	63.5	3.00E−12	25%	43%	1%	2.32
3SIO_B	63.5	3.00E−12	25%	43%	1%	2.32
3SIO_C	63.5	3.00E−12	25%	43%	1%	2.32
3SIO_D	63.5	3.00E−12	25%	43%	1%	2.32
3SIO_E	63.5	3.00E−12	25%	43%	1%	2.32
3SIO_F	63.5	3.00E−12	25%	43%	1%	2.32
3SIO_G	63.5	3.00E−12	25%	43%	1%	2.32
3SIO_H	63.5	3.00E−12	25%	43%	1%	2.32

Continued

3SIO_I	63.5	3.00E−12	25%	43%	1%	2.32
3SIO_J	63.5	3.00E−12	25%	43%	1%	2.32
3U8J_A	44.3	2.20E−05	24%	40%	3%	2.35
3U8J_B	44.3	2.20E−05	24%	40%	3%	2.35
3U8J_C	44.3	2.20E−05	24%	40%	3%	2.35
3U8J_D	44.3	2.20E−05	24%	40%	3%	2.35
3U8J_E	44.3	2.20E−05	24%	40%	3%	2.35
3U8J_F	44.3	2.20E−05	24%	40%	3%	2.35
3U8J_G	44.3	2.20E−05	24%	40%	3%	2.35
3U8J_H	44.3	2.20E−05	24%	40%	3%	2.35
3U8J_I	44.3	2.20E−05	24%	40%	3%	2.35
3U8J_J	44.3	2.20E−05	24%	40%	3%	2.35
3U8N_A	44.3	2.20E−05	24%	40%	3%	2.35
3U8N_B	44.3	2.20E−05	24%	40%	3%	2.35
3U8N_C	44.3	2.20E−05	24%	40%	3%	2.35
3U8N_D	44.3	2.20E−05	24%	40%	3%	2.35
3U8N_E	44.3	2.20E−05	24%	40%	3%	2.35
3U8N_F	44.3	2.20E−05	24%	40%	3%	2.35
3U8N_G	44.3	2.20E−05	24%	40%	3%	2.35
3U8N_H	44.3	2.20E−05	24%	40%	3%	2.35
3U8N_I	44.3	2.20E−05	24%	40%	3%	2.35
3U8N_J	44.3	2.20E−05	24%	40%	3%	2.35
3U8N_K	44.3	2.20E−05	24%	40%	3%	2.35
3U8N_L	44.3	2.20E−05	24%	40%	3%	2.35
3U8N_M	44.3	2.20E−05	24%	40%	3%	2.35
3U8N_N	44.3	2.20E−05	24%	40%	3%	2.35
3U8N_O	44.3	2.20E−05	24%	40%	3%	2.35
3U8N_P	44.3	2.20E−05	24%	40%	3%	2.35
3U8N_Q	44.3	2.20E−05	24%	40%	3%	2.35
3U8N_R	44.3	2.20E−05	24%	40%	3%	2.35
3U8N_S	44.3	2.20E−05	24%	40%	3%	2.35
3U8N_T	44.3	2.20E−05	24%	40%	3%	2.35
2X00_A	63.5	2.20E−12	24%	44%	4%	2.4
2X00_B	63.5	2.20E−12	24%	44%	4%	2.4
2X00_C	63.5	2.20E−12	24%	44%	4%	2.4
2X00_D	63.5	2.20E−12	24%	44%	4%	2.4
2X00_E	63.5	2.20E−12	24%	44%	4%	2.4

Continued

2BR8_A	63.9	1.50E−12	25%	45%	4%	2.4
2BR8_B	63.9	1.50E−12	25%	45%	4%	2.4
2BR8_C	63.9	1.50E−12	25%	45%	4%	2.4
2BR8_D	63.9	1.50E−12	25%	45%	4%	2.4
2BR8_E	63.9	1.50E−12	25%	45%	4%	2.4
2UZ6_A	63.9	1.50E−12	25%	45%	4%	2.4
2UZ6_B	63.9	1.50E−12	25%	45%	4%	2.4
2UZ6_C	63.9	1.50E−12	25%	45%	4%	2.4
2UZ6_D	63.9	1.50E−12	25%	45%	4%	2.4
2UZ6_E	63.9	1.50E−12	25%	45%	4%	2.4
2UZ6_F	63.9	1.50E−12	25%	45%	4%	2.4
2UZ6_G	63.9	1.50E−12	25%	45%	4%	2.4
2UZ6_H	63.9	1.50E−12	25%	45%	4%	2.4
2UZ6_I	63.9	1.50E−12	25%	45%	4%	2.4
2UZ6_J	63.9	1.50E−12	25%	45%	4%	2.4
2YME_A	66.6	1.60E−13	25%	43%	1%	2.4
2YME_B	66.6	1.60E−13	25%	43%	1%	2.4
2YME_C	66.6	1.60E−13	25%	43%	1%	2.4
2YME_D	66.6	1.60E−13	25%	43%	1%	2.4
2YME_E	66.6	1.60E−13	25%	43%	1%	2.4
2YME_F	66.6	1.60E−13	25%	43%	1%	2.4
2YME_G	66.6	1.60E−13	25%	43%	1%	2.4
2YME_H	66.6	1.60E−13	25%	43%	1%	2.4
2YME_I	66.6	1.60E−13	25%	43%	1%	2.4
2YME_J	66.6	1.60E−13	25%	43%	1%	2.4
2XNV_A	63.5	2.80E−12	24%	44%	4%	2.44
2XNV_B	63.5	2.80E−12	24%	44%	4%	2.44
2XNV_C	63.5	2.80E−12	24%	44%	4%	2.44
2XNV_D	63.5	2.80E−12	24%	44%	4%	2.44
2XNV_E	63.5	2.80E−12	24%	44%	4%	2.44
2XNV_F	63.5	2.80E−12	24%	44%	4%	2.44
2XNV_G	63.5	2.80E−12	24%	44%	4%	2.44
2XNV_H	63.5	2.80E−12	24%	44%	4%	2.44
2XNV_I	63.5	2.80E−12	24%	44%	4%	2.44
2XNV_J	63.5	2.80E−12	24%	44%	4%	2.44
3PMZ_A	63.5	2.60E−12	24%	44%	4%	2.44
3PMZ_B	63.5	2.60E−12	24%	44%	4%	2.44

Continued

3PMZ_C	63.5	2.60E−12	24%	44%	4%	2.44
3PMZ_D	63.5	2.60E−12	24%	44%	4%	2.44
3PMZ_E	63.5	2.60E−12	24%	44%	4%	2.44
3PMZ_F	63.5	2.60E−12	24%	44%	4%	2.44
3PMZ_G	63.5	2.60E−12	24%	44%	4%	2.44
3PMZ_H	63.5	2.60E−12	24%	44%	4%	2.44
3PMZ_I	63.5	2.60E−12	24%	44%	4%	2.44
3PMZ_J	63.5	2.60E−12	24%	44%	4%	2.44
2BYR_A	63.5	2.60E−12	24%	44%	4%	2.45
2BYR_B	63.5	2.60E−12	24%	44%	4%	2.45
2BYR_C	63.5	2.60E−12	24%	44%	4%	2.45
2BYR_D	63.5	2.60E−12	24%	44%	4%	2.45
2BYR_E	63.5	2.60E−12	24%	44%	4%	2.45
2BYR_F	63.5	2.60E−12	24%	44%	4%	2.45
2BYR_G	63.5	2.60E−12	24%	44%	4%	2.45
2BYR_H	63.5	2.60E−12	24%	44%	4%	2.45
2BYR_I	63.5	2.60E−12	24%	44%	4%	2.45
2BYR_J	63.5	2.60E−12	24%	44%	4%	2.45
3U8K_A	44.3	2.20E−05	24%	40%	3%	2.47
3U8K_B	44.3	2.20E−05	24%	40%	3%	2.47
3U8K_C	44.3	2.20E−05	24%	40%	3%	2.47
3U8K_D	44.3	2.20E−05	24%	40%	3%	2.47
3U8K_E	44.3	2.20E−05	24%	40%	3%	2.47
3U8K_F	44.3	2.20E−05	24%	40%	3%	2.47
3U8K_G	44.3	2.20E−05	24%	40%	3%	2.47
3U8K_H	44.3	2.20E−05	24%	40%	3%	2.47
3U8K_I	44.3	2.20E−05	24%	40%	3%	2.47
3U8K_J	44.3	2.20E−05	24%	40%	3%	2.47
3U8K_K	44.3	2.20E−05	24%	40%	3%	2.47
3U8K_L	44.3	2.20E−05	24%	40%	3%	2.47
3U8K_M	44.3	2.20E−05	24%	40%	3%	2.47
3U8K_N	44.3	2.20E−05	24%	40%	3%	2.47
3U8K_O	44.3	2.20E−05	24%	40%	3%	2.47
3U8K_P	44.3	2.20E−05	24%	40%	3%	2.47
3U8K_Q	44.3	2.20E−05	24%	40%	3%	2.47
3U8K_R	44.3	2.20E−05	24%	40%	3%	2.47
3U8K_S	44.3	2.20E−05	24%	40%	3%	2.47

Continued

3U8K_T	44.3	2.20E−05	24%	40%	3%	2.47
3C79_A	63.5	2.60E−12	24%	44%	4%	2.48
3C79_B	63.5	2.60E−12	24%	44%	4%	2.48
3C79_C	63.5	2.60E−12	24%	44%	4%	2.48
3C79_D	63.5	2.60E−12	24%	44%	4%	2.48
3C79_E	63.5	2.60E−12	24%	44%	4%	2.48
1UV6_A	44.3	2.20E−05	24%	40%	3%	2.5
1UV6_B	44.3	2.20E−05	24%	40%	3%	2.5
1UV6_C	44.3	2.20E−05	24%	40%	3%	2.5
1UV6_D	44.3	2.20E−05	24%	40%	3%	2.5
1UV6_E	44.3	2.20E−05	24%	40%	3%	2.5
1UV6_F	44.3	2.20E−05	24%	40%	3%	2.5
1UV6_G	44.3	2.20E−05	24%	40%	3%	2.5
1UV6_H	44.3	2.20E−05	24%	40%	3%	2.5
1UV6_I	44.3	2.20E−05	24%	40%	3%	2.5
1UV6_J	44.3	2.20E−05	24%	40%	3%	2.5
3C75_L	29.6	1.4	29%	43%	0%	2.5
3C75_M	29.6	1.4	29%	43%	0%	2.5
2WZY_A	63.5	2.20E−12	24%	44%	4%	2.51
2WZY_B	63.5	2.20E−12	24%	44%	4%	2.51
2WZY_C	63.5	2.20E−12	24%	44%	4%	2.51
2WZY_D	63.5	2.20E−12	24%	44%	4%	2.51
2WZY_E	63.5	2.20E−12	24%	44%	4%	2.51
2WZY_F	63.5	2.20E−12	24%	44%	4%	2.51
2WZY_G	63.5	2.20E−12	24%	44%	4%	2.51
2WZY_H	63.5	2.20E−12	24%	44%	4%	2.51
2WZY_I	63.5	2.20E−12	24%	44%	4%	2.51
2WZY_J	63.5	2.20E−12	24%	44%	4%	2.51
2XNU_A	63.5	2.80E−12	24%	44%	4%	2.55
2XNU_B	63.5	2.80E−12	24%	44%	4%	2.55
2XNU_C	63.5	2.80E−12	24%	44%	4%	2.55
2XNU_D	63.5	2.80E−12	24%	44%	4%	2.55
2XNU_E	63.5	2.80E−12	24%	44%	4%	2.55
2ZJU_A	43.9	2.90E−05	24%	41%	3%	2.58
2ZJU_B	43.9	2.90E−05	24%	41%	3%	2.58
2ZJU_C	43.9	2.90E−05	24%	41%	3%	2.58
2ZJU_D	43.9	2.90E−05	24%	41%	3%	2.58

Continued

2ZJU_E	43.9	2.90E−05	24%	41%	3%	2.58
3TLW_A	40	0.00074	24%	42%	7%	2.6
3TLW_B	40	0.00074	24%	42%	7%	2.6
3TLW_C	40	0.00074	24%	42%	7%	2.6
3TLW_D	40	0.00074	24%	42%	7%	2.6
3TLW_E	40	0.00074	24%	42%	7%	2.6
2W8G_A	63.9	1.50E−12	25%	45%	4%	2.6
2W8G_B	63.9	1.50E−12	25%	45%	4%	2.6
2W8G_C	63.9	1.50E−12	25%	45%	4%	2.6
2W8G_D	63.9	1.50E−12	25%	45%	4%	2.6
2W8G_E	63.9	1.50E−12	25%	45%	4%	2.6
1I9B_A	43.9	2.70E−05	24%	40%	3%	2.7
1I9B_B	43.9	2.70E−05	24%	40%	3%	2.7
1I9B_C	43.9	2.70E−05	24%	40%	3%	2.7
1I9B_D	43.9	2.70E−05	24%	40%	3%	2.7
1I9B_E	43.9	2.70E−05	24%	40%	3%	2.7
2WNL_A	63.5	2.60E−12	24%	44%	4%	2.7
2WNL_B	63.5	2.60E−12	24%	44%	4%	2.7
2WNL_C	63.5	2.60E−12	24%	44%	4%	2.7
2WNL_D	63.5	2.60E−12	24%	44%	4%	2.7
2WNL_E	63.5	2.60E−12	24%	44%	4%	2.7
2WNL_F	63.5	2.60E−12	24%	44%	4%	2.7
2WNL_G	63.5	2.60E−12	24%	44%	4%	2.7
2WNL_H	63.5	2.60E−12	24%	44%	4%	2.7
2WNL_I	63.5	2.60E−12	24%	44%	4%	2.7
2WNL_J	63.5	2.60E−12	24%	44%	4%	2.7
2ZJV_A	43.9	2.90E−05	24%	41%	3%	2.7
2ZJV_B	43.9	2.90E−05	24%	41%	3%	2.7
2ZJV_C	43.9	2.90E−05	24%	41%	3%	2.7
2ZJV_D	43.9	2.90E−05	24%	41%	3%	2.7
2ZJV_E	43.9	2.90E−05	24%	41%	3%	2.7
3U8M_A	44.3	2.20E−05	24%	40%	3%	2.7
3U8M_B	44.3	2.20E−05	24%	40%	3%	2.7
3U8M_C	44.3	2.20E−05	24%	40%	3%	2.7
3U8M_D	44.3	2.20E−05	24%	40%	3%	2.7
3U8M_E	44.3	2.20E−05	24%	40%	3%	2.7
3U8M_F	44.3	2.20E−05	24%	40%	3%	2.7

Continued

3U8M_G	44.3	2.20E−05	24%	40%	3%	2.7
3U8M_H	44.3	2.20E−05	24%	40%	3%	2.7
3U8M_I	44.3	2.20E−05	24%	40%	3%	2.7
3U8M_J	44.3	2.20E−05	24%	40%	3%	2.7
3U8M_K	44.3	2.20E−05	24%	40%	3%	2.7
3U8M_L	44.3	2.20E−05	24%	40%	3%	2.7
3U8M_M	44.3	2.20E−05	24%	40%	3%	2.7
3U8M_N	44.3	2.20E−05	24%	40%	3%	2.7
3U8M_O	44.3	2.20E−05	24%	40%	3%	2.7
3U8M_P	44.3	2.20E−05	24%	40%	3%	2.7
3U8M_Q	44.3	2.20E−05	24%	40%	3%	2.7
3U8M_R	44.3	2.20E−05	24%	40%	3%	2.7
3U8M_S	44.3	2.20E−05	24%	40%	3%	2.7
3U8M_T	44.3	2.20E−05	24%	40%	3%	2.7
2W8F_A	63.9	1.50E−12	25%	45%	4%	2.7
2W8F_B	63.9	1.50E−12	25%	45%	4%	2.7
2W8F_C	63.9	1.50E−12	25%	45%	4%	2.7
2W8F_D	63.9	1.50E−12	25%	45%	4%	2.7
2W8F_E	63.9	1.50E−12	25%	45%	4%	2.7
2W8F_F	63.9	1.50E−12	25%	45%	4%	2.7
2W8F_G	63.9	1.50E−12	25%	45%	4%	2.7
2W8F_H	63.9	1.50E−12	25%	45%	4%	2.7
2W8F_I	63.9	1.50E−12	25%	45%	4%	2.7
2W8F_J	63.9	1.50E−12	25%	45%	4%	2.7
2XZ5_A	62.4	5.50E−12	25%	44%	4%	2.8
2XZ5_B	62.4	5.50E−12	25%	44%	4%	2.8
2XZ5_C	62.4	5.50E−12	25%	44%	4%	2.8
2XZ5_D	62.4	5.50E−12	25%	44%	4%	2.8
2XZ5_E	62.4	5.50E−12	25%	44%	4%	2.8
3SQ6_A	85.1	6.50E−20	28%	48%	4%	2.8
3SQ6_B	85.1	6.50E−20	28%	48%	4%	2.8
3SQ6_C	85.1	6.50E−20	28%	48%	4%	2.8
3SQ6_D	85.1	6.50E−20	28%	48%	4%	2.8
3SQ6_E	85.1	6.50E−20	28%	48%	4%	2.8
3SQ6_F	85.1	6.50E−20	28%	48%	4%	2.8
3SQ6_G	85.1	6.50E−20	28%	48%	4%	2.8
3SQ6_H	85.1	6.50E−20	28%	48%	4%	2.8

Continued

3SQ6_I	85.1	6.50E−20	28%	48%	4%	2.8
3SQ6_J	85.1	6.50E−20	28%	48%	4%	2.8
3TLU_A	40	0.00074	24%	42%	7%	2.85
3TLU_B	40	0.00074	24%	42%	7%	2.85
3TLU_C	40	0.00074	24%	42%	7%	2.85
3TLU_D	40	0.00074	24%	42%	7%	2.85
3TLU_E	40	0.00074	24%	42%	7%	2.85
2PH9_A	63.5	2.30E−12	24%	44%	4%	2.88
2PH9_B	63.5	2.30E−12	24%	44%	4%	2.88
2PH9_C	63.5	2.30E−12	24%	44%	4%	2.88
2PH9_D	63.5	2.30E−12	24%	44%	4%	2.88
2PH9_E	63.5	2.30E−12	24%	44%	4%	2.88
3EAM_A	42.7	9.30E−05	24%	43%	7%	2.9
3EAM_B	42.7	9.30E−05	24%	43%	7%	2.9
3EAM_C	42.7	9.30E−05	24%	43%	7%	2.9
3EAM_D	42.7	9.30E−05	24%	43%	7%	2.9
3EAM_E	42.7	9.30E−05	24%	43%	7%	2.9
3TLV_A	40	0.00068	24%	42%	7%	2.9
3TLV_B	40	0.00068	24%	42%	7%	2.9
3TLV_C	40	0.00068	24%	42%	7%	2.9
3TLV_D	40	0.00068	24%	42%	7%	2.9
3TLV_E	40	0.00068	24%	42%	7%	2.9
3UU5_A	40	0.0007	24%	42%	7%	2.9
3UU5_B	40	0.0007	24%	42%	7%	2.9
3UU5_C	40	0.0007	24%	42%	7%	2.9
3UU5_D	40	0.0007	24%	42%	7%	2.9
3UU5_E	40	0.0007	24%	42%	7%	2.9
3UUB_A	40	0.00074	24%	42%	7%	2.9
3UUB_B	40	0.00074	24%	42%	7%	2.9
3UUB_C	40	0.00074	24%	42%	7%	2.9
3UUB_D	40	0.00074	24%	42%	7%	2.9
3UUB_E	40	0.00074	24%	42%	7%	2.9
3UUB_F	40	0.00074	24%	42%	7%	2.9
3UUB_G	40	0.00074	24%	42%	7%	2.9
3UUB_H	40	0.00074	24%	42%	7%	2.9
3UUB_I	40	0.00074	24%	42%	7%	2.9
3UUB_J	40	0.00074	24%	42%	7%	2.9

Continued

3SH1_A	65.5	4.80E−13	25%	43%	1%	2.9
3SH1_B	65.5	4.80E−13	25%	43%	1%	2.9
3SH1_C	65.5	4.80E−13	25%	43%	1%	2.9
3SH1_D	65.5	4.80E−13	25%	43%	1%	2.9
3SH1_E	65.5	4.80E−13	25%	43%	1%	2.9
3SH1_F	65.5	4.80E−13	25%	43%	1%	2.9
3SH1_G	65.5	4.80E−13	25%	43%	1%	2.9
3SH1_H	65.5	4.80E−13	25%	43%	1%	2.9
3SH1_I	65.5	4.80E−13	25%	43%	1%	2.9
3SH1_J	65.5	4.80E−13	25%	43%	1%	2.9
3RQW_A	27.3	9	18%	42%	10%	2.91
3RQW_B	27.3	9	18%	42%	10%	2.91
3RQW_C	27.3	9	18%	42%	10%	2.91
3RQW_D	27.3	9	18%	42%	10%	2.91
3RQW_E	27.3	9	18%	42%	10%	2.91
3RQW_F	27.3	9	18%	42%	10%	2.91
3RQW_G	27.3	9	18%	42%	10%	2.91
3RQW_H	27.3	9	18%	42%	10%	2.91
3RQW_I	27.3	9	18%	42%	10%	2.91
3RQW_J	27.3	9	18%	42%	10%	2.91
3UU6_A	40	0.00068	24%	42%	7%	2.98
3UU6_B	40	0.00068	24%	42%	7%	2.98
3UU6_C	40	0.00068	24%	42%	7%	2.98
3UU6_D	40	0.00068	24%	42%	7%	2.98
3UU6_E	40	0.00068	24%	42%	7%	2.98
4F8H_A	42.7	8.70E−05	24%	43%	7%	2.99
4F8H_B	42.7	8.70E−05	24%	43%	7%	2.99
4F8H_C	42.7	8.70E−05	24%	43%	7%	2.99
4F8H_D	42.7	8.70E−05	24%	43%	7%	2.99
4F8H_E	42.7	8.70E−05	24%	43%	7%	2.99
2BR7_A	63.9	1.50E−12	25%	45%	4%	3
2BR7_B	63.9	1.50E−12	25%	45%	4%	3
2BR7_C	63.9	1.50E−12	25%	45%	4%	3
2BR7_D	63.9	1.50E−12	25%	45%	4%	3
2BR7_E	63.9	1.50E−12	25%	45%	4%	3
3T4M_A	69.7	2.00E−14	26%	44%	1%	3
3T4M_B	69.7	2.00E−14	26%	44%	1%	3

Continued

3T4M_C	69.7	2.00E−14	26%	44%	1%	3
3T4M_D	69.7	2.00E−14	26%	44%	1%	3
3T4M_E	69.7	2.00E−14	26%	44%	1%	3
3T4M_F	69.7	2.00E−14	26%	44%	1%	3
3T4M_G	69.7	2.00E−14	26%	44%	1%	3
3T4M_H	69.7	2.00E−14	26%	44%	1%	3
3T4M_I	69.7	2.00E−14	26%	44%	1%	3
3T4M_J	69.7	2.00E−14	26%	44%	1%	3
1LDJ_A	28.1	7.2	29%	50%	15%	3
3UU4_A	40	0.00074	24%	42%	7%	3.05
3UU4_B	40	0.00074	24%	42%	7%	3.05
3UU4_C	40	0.00074	24%	42%	7%	3.05
3UU4_D	40	0.00074	24%	42%	7%	3.05
3UU4_E	40	0.00074	24%	42%	7%	3.05
3RQU_A	27.3	9	18%	42%	10%	3.09
3RQU_B	27.3	9	18%	42%	10%	3.09
3RQU_C	27.3	9	18%	42%	10%	3.09
3RQU_D	27.3	9	18%	42%	10%	3.09
3RQU_E	27.3	9	18%	42%	10%	3.09
3RQU_F	27.3	9	18%	42%	10%	3.09
3RQU_G	27.3	9	18%	42%	10%	3.09
3RQU_H	27.3	9	18%	42%	10%	3.09
3RQU_I	27.3	9	18%	42%	10%	3.09
3RQU_J	27.3	9	18%	42%	10%	3.09
3EHZ_A	42.7	8.70E−05	24%	43%	7%	3.1
3EHZ_B	42.7	8.70E−05	24%	43%	7%	3.1
3EHZ_C	42.7	8.70E−05	24%	43%	7%	3.1
3EHZ_D	42.7	8.70E−05	24%	43%	7%	3.1
3EHZ_E	42.7	8.70E−05	24%	43%	7%	3.1
3GUA_A	63.5	2.30E−12	24%	43%	1%	3.1
3GUA_B	63.5	2.30E−12	24%	43%	1%	3.1
3GUA_C	63.5	2.30E−12	24%	43%	1%	3.1
3GUA_D	63.5	2.30E−12	24%	43%	1%	3.1
3GUA_E	63.5	2.30E−12	24%	43%	1%	3.1
3GUA_F	63.5	2.30E−12	24%	43%	1%	3.1
3GUA_G	63.5	2.30E−12	24%	43%	1%	3.1
3GUA_H	63.5	2.30E−12	24%	43%	1%	3.1

Continued

3GUA_I	63.5	2.30E−12	24%	43%	1%	3.1
3GUA_J	63.5	2.30E−12	24%	43%	1%	3.1
3SQ9_A	85.1	6.50E−20	28%	48%	4%	3.1
3SQ9_B	85.1	6.50E−20	28%	48%	4%	3.1
3SQ9_C	85.1	6.50E−20	28%	48%	4%	3.1
3SQ9_D	85.1	6.50E−20	28%	48%	4%	3.1
3SQ9_E	85.1	6.50E−20	28%	48%	4%	3.1
3SQ9_F	85.1	6.50E−20	28%	48%	4%	3.1
3SQ9_G	85.1	6.50E−20	28%	48%	4%	3.1
3SQ9_H	85.1	6.50E−20	28%	48%	4%	3.1
3SQ9_I	85.1	6.50E−20	28%	48%	4%	3.1
3SQ9_J	85.1	6.50E−20	28%	48%	4%	3.1
1LDK_A	28.5	4.9	29%	50%	15%	3.1
1U6G_A	28.1	7.2	29%	50%	15%	3.1
2XZ6_A	62.8	4.70E−12	25%	44%	4%	3.137
2XZ6_B	62.8	4.70E−12	25%	44%	4%	3.137
2XZ6_C	62.8	4.70E−12	25%	44%	4%	3.137
2XZ6_D	62.8	4.70E−12	25%	44%	4%	3.137
2XZ6_E	62.8	4.70E−12	25%	44%	4%	3.137
2XZ6_F	62.8	4.70E−12	25%	44%	4%	3.137
2XZ6_G	62.8	4.70E−12	25%	44%	4%	3.137
2XZ6_H	62.8	4.70E−12	25%	44%	4%	3.137
2XZ6_I	62.8	4.70E−12	25%	44%	4%	3.137
2XZ6_J	62.8	4.70E−12	25%	44%	4%	3.137
3LSV_A	42.7	9.60E−05	24%	43%	7%	3.15
3LSV_B	42.7	9.60E−05	24%	43%	7%	3.15
3LSV_C	42.7	9.60E−05	24%	43%	7%	3.15
3LSV_D	42.7	9.60E−05	24%	43%	7%	3.15
3LSV_E	42.7	9.60E−05	24%	43%	7%	3.15
3UU3_A	40	0.0007	24%	42%	7%	3.15
3UU3_B	40	0.0007	24%	42%	7%	3.15
3UU3_C	40	0.0007	24%	42%	7%	3.15
3UU3_D	40	0.0007	24%	42%	7%	3.15
3UU3_E	40	0.0007	24%	42%	7%	3.15
2XQ9_A	42.7	8.60E−05	24%	43%	7%	3.2
2XQ9_B	42.7	8.60E−05	24%	43%	7%	3.2
2XQ9_C	42.7	8.60E−05	24%	43%	7%	3.2

Continued

2XQ9_D	42.7	8.60E−05	24%	43%	7%	3.2
2XQ9_E	42.7	8.60E−05	24%	43%	7%	3.2
3P4W_A	42.7	8.60E−05	24%	43%	7%	3.2
3P4W_B	42.7	8.60E−05	24%	43%	7%	3.2
3P4W_C	42.7	8.60E−05	24%	43%	7%	3.2
3P4W_D	42.7	8.60E−05	24%	43%	7%	3.2
3P4W_E	42.7	8.60E−05	24%	43%	7%	3.2
3TLS_A	42.7	9.00E−05	24%	43%	7%	3.2
3TLS_B	42.7	9.00E−05	24%	43%	7%	3.2
3TLS_C	42.7	9.00E−05	24%	43%	7%	3.2
3TLS_D	42.7	9.00E−05	24%	43%	7%	3.2
3TLS_E	42.7	9.00E−05	24%	43%	7%	3.2
4AFT_A	63.9	1.50E−12	25%	45%	4%	3.2
4AFT_B	63.9	1.50E−12	25%	45%	4%	3.2
4AFT_C	63.9	1.50E−12	25%	45%	4%	3.2
4AFT_D	63.9	1.50E−12	25%	45%	4%	3.2
4AFT_E	63.9	1.50E−12	25%	45%	4%	3.2
2XNT_A	63.5	2.80E−12	24%	44%	4%	3.21
2XNT_B	63.5	2.80E−12	24%	44%	4%	3.21
2XNT_C	63.5	2.80E−12	24%	44%	4%	3.21
2XNT_D	63.5	2.80E−12	24%	44%	4%	3.21
2XNT_E	63.5	2.80E−12	24%	44%	4%	3.21
2XNT_F	63.5	2.80E−12	24%	44%	4%	3.21
2XNT_G	63.5	2.80E−12	24%	44%	4%	3.21
2XNT_H	63.5	2.80E−12	24%	44%	4%	3.21
2XNT_I	63.5	2.80E−12	24%	44%	4%	3.21
2XNT_J	63.5	2.80E−12	24%	44%	4%	3.21
3UU8_A	40	0.00074	24%	42%	7%	3.25
3UU8_B	40	0.00074	24%	42%	7%	3.25
3UU8_C	40	0.00074	24%	42%	7%	3.25
3UU8_D	40	0.00074	24%	42%	7%	3.25
3UU8_E	40	0.00074	24%	42%	7%	3.25
2Y58_A	63.9	1.50E−12	25%	45%	4%	3.25
2Y58_B	63.9	1.50E−12	25%	45%	4%	3.25
2Y58_C	63.9	1.50E−12	25%	45%	4%	3.25
2Y58_D	63.9	1.50E−12	25%	45%	4%	3.25
2Y58_E	63.9	1.50E−12	25%	45%	4%	3.25

Continued

3RHW_A	46.2	6.90E−06	22%	44%	4%	3.26
3RHW_B	46.2	6.90E−06	22%	44%	4%	3.26
3RHW_C	46.2	6.90E−06	22%	44%	4%	3.26
3RHW_D	46.2	6.90E−06	22%	44%	4%	3.26
3RHW_E	46.2	6.90E−06	22%	44%	4%	3.26
2VL0_A	27.3	9.7	18%	42%	10%	3.3
2VL0_B	27.3	9.7	18%	42%	10%	3.3
2VL0_C	27.3	9.7	18%	42%	10%	3.3
2VL0_D	27.3	9.7	18%	42%	10%	3.3
2VL0_E	27.3	9.7	18%	42%	10%	3.3
2VL0_F	27.3	9.7	18%	42%	10%	3.3
2VL0_G	27.3	9.7	18%	42%	10%	3.3
2VL0_H	27.3	9.7	18%	42%	10%	3.3
2VL0_I	27.3	9.7	18%	42%	10%	3.3
2VL0_J	27.3	9.7	18%	42%	10%	3.3
2YKS_A	27.3	9.8	18%	42%	10%	3.3
2YKS_B	27.3	9.8	18%	42%	10%	3.3
2YKS_C	27.3	9.8	18%	42%	10%	3.3
2YKS_D	27.3	9.8	18%	42%	10%	3.3
2YKS_E	27.3	9.8	18%	42%	10%	3.3
2YKS_F	27.3	9.8	18%	42%	10%	3.3
2YKS_G	27.3	9.8	18%	42%	10%	3.3
2YKS_H	27.3	9.8	18%	42%	10%	3.3
2YKS_I	27.3	9.8	18%	42%	10%	3.3
2YKS_J	27.3	9.8	18%	42%	10%	3.3
3P50_A	42.7	8.60E−05	24%	43%	7%	3.3
3P50_B	42.7	8.60E−05	24%	43%	7%	3.3
3P50_C	42.7	8.60E−05	24%	43%	7%	3.3
3P50_D	42.7	8.60E−05	24%	43%	7%	3.3
3P50_E	42.7	8.60E−05	24%	43%	7%	3.3
3TLT_A	42.7	0.0001	24%	43%	7%	3.3
3TLT_B	42.7	0.0001	24%	43%	7%	3.3
3TLT_C	42.7	0.0001	24%	43%	7%	3.3
3TLT_D	42.7	0.0001	24%	43%	7%	3.3
3TLT_E	42.7	0.0001	24%	43%	7%	3.3
2Y57_A	63.9	1.50E−12	25%	45%	4%	3.3
2Y57_B	63.9	1.50E−12	25%	45%	4%	3.3

Continued

2Y57_C	63.9	1.50E−12	25%	45%	4%	3.3
2Y57_D	63.9	1.50E−12	25%	45%	4%	3.3
2Y57_E	63.9	1.50E−12	25%	45%	4%	3.3
2YN6_A	27.3	9	18%	42%	10%	3.31
2YN6_B	27.3	9	18%	42%	10%	3.31
2YN6_C	27.3	9	18%	42%	10%	3.31
2YN6_D	27.3	9	18%	42%	10%	3.31
2YN6_E	27.3	9	18%	42%	10%	3.31
3RIF_A	46.2	6.90E−06	22%	44%	4%	3.35
3RIF_B	46.2	6.90E−06	22%	44%	4%	3.35
3RIF_C	46.2	6.90E−06	22%	44%	4%	3.35
3RIF_D	46.2	6.90E−06	22%	44%	4%	3.35
3RIF_E	46.2	6.90E−06	22%	44%	4%	3.35
3RI5_A	46.2	6.90E−06	22%	44%	4%	3.4
3RI5_B	46.2	6.90E−06	22%	44%	4%	3.4
3RI5_C	46.2	6.90E−06	22%	44%	4%	3.4
3RI5_D	46.2	6.90E−06	22%	44%	4%	3.4
3RI5_E	46.2	6.90E−06	22%	44%	4%	3.4
2BYQ_A	63.5	2.60E−12	24%	44%	4%	3.4
2BYQ_B	63.5	2.60E−12	24%	44%	4%	3.4
2BYQ_C	63.5	2.60E−12	24%	44%	4%	3.4
2BYQ_D	63.5	2.60E−12	24%	44%	4%	3.4
2BYQ_E	63.5	2.60E−12	24%	44%	4%	3.4
2XQ7_A	42.7	8.70E−05	24%	43%	7%	3.4
2XQ7_B	42.7	8.70E−05	24%	43%	7%	3.4
2XQ7_C	42.7	8.70E−05	24%	43%	7%	3.4
2XQ7_D	42.7	8.70E−05	24%	43%	7%	3.4
2XQ7_E	42.7	8.70E−05	24%	43%	7%	3.4
3UQ4_A	27.3	8.9	18%	42%	10%	3.5
3UQ4_B	27.3	8.9	18%	42%	10%	3.5
3UQ4_C	27.3	8.9	18%	42%	10%	3.5
3UQ4_D	27.3	8.9	18%	42%	10%	3.5
3UQ4_E	27.3	8.9	18%	42%	10%	3.5
3UQ4_F	27.3	8.9	18%	42%	10%	3.5
3UQ4_G	27.3	8.9	18%	42%	10%	3.5
3UQ4_H	27.3	8.9	18%	42%	10%	3.5
3UQ4_I	27.3	8.9	18%	42%	10%	3.5

Continued

3UQ4_J	27.3	8.9	18%	42%	10%	3.5
2XQ3_A	42.7	8.70E−05	24%	43%	7%	3.5
2XQ3_B	42.7	8.70E−05	24%	43%	7%	3.5
2XQ3_C	42.7	8.70E−05	24%	43%	7%	3.5
2XQ3_D	42.7	8.70E−05	24%	43%	7%	3.5
2XQ3_E	42.7	8.70E−05	24%	43%	7%	3.5
2XQ5_A	42.7	8.70E−05	24%	43%	7%	3.5
2XQ5_B	42.7	8.70E−05	24%	43%	7%	3.5
2XQ5_C	42.7	8.70E−05	24%	43%	7%	3.5
2XQ5_D	42.7	8.70E−05	24%	43%	7%	3.5
2XQ5_E	42.7	8.70E−05	24%	43%	7%	3.5
3EI0_A	42.7	9.00E−05	24%	43%	7%	3.5
3EI0_B	42.7	9.00E−05	24%	43%	7%	3.5
3EI0_C	42.7	9.00E−05	24%	43%	7%	3.5
3EI0_D	42.7	9.00E−05	24%	43%	7%	3.5
3EI0_E	42.7	9.00E−05	24%	43%	7%	3.5
2Y56_A	63.9	1.50E−12	25%	45%	4%	3.59
2Y56_B	63.9	1.50E−12	25%	45%	4%	3.59
2Y56_C	63.9	1.50E−12	25%	45%	4%	3.59
2Y56_D	63.9	1.50E−12	25%	45%	4%	3.59
2Y56_E	63.9	1.50E−12	25%	45%	4%	3.59
2XQ4_A	42.7	8.70E−05	24%	43%	7%	3.6
2XQ4_B	42.7	8.70E−05	24%	43%	7%	3.6
2XQ4_C	42.7	8.70E−05	24%	43%	7%	3.6
2XQ4_D	42.7	8.70E−05	24%	43%	7%	3.6
2XQ4_E	42.7	8.70E−05	24%	43%	7%	3.6
2XQ8_A	42.7	8.70E−05	24%	43%	7%	3.6
2XQ8_B	42.7	8.70E−05	24%	43%	7%	3.6
2XQ8_C	42.7	8.70E−05	24%	43%	7%	3.6
2XQ8_D	42.7	8.70E−05	24%	43%	7%	3.6
2XQ8_E	42.7	8.70E−05	24%	43%	7%	3.6
2Y54_A	63.9	1.50E−12	25%	45%	4%	3.65
2Y54_B	63.9	1.50E−12	25%	45%	4%	3.65
2Y54_C	63.9	1.50E−12	25%	45%	4%	3.65

Continued

2Y54_D	63.9	1.50E−12	25%	45%	4%	3.65
2Y54_E	63.9	1.50E−12	25%	45%	4%	3.65
2XQ6_A	42.7	8.70E−05	24%	43%	7%	3.7
2XQ6_B	42.7	8.70E−05	24%	43%	7%	3.7
2XQ6_C	42.7	8.70E−05	24%	43%	7%	3.7
2XQ6_D	42.7	8.70E−05	24%	43%	7%	3.7
2XQ6_E	42.7	8.70E−05	24%	43%	7%	3.7
2XQA_A	42.7	8.70E−05	24%	43%	7%	3.7
2XQA_B	42.7	8.70E−05	24%	43%	7%	3.7
2XQA_C	42.7	8.70E−05	24%	43%	7%	3.7
2XQA_D	42.7	8.70E−05	24%	43%	7%	3.7
2XQA_E	42.7	8.70E−05	24%	43%	7%	3.7
3UQ7_A	27.3	9.4	18%	42%	10%	3.8
3UQ7_B	27.3	9.4	18%	42%	10%	3.8
3UQ7_C	27.3	9.4	18%	42%	10%	3.8
3UQ7_D	27.3	9.4	18%	42%	10%	3.8
3UQ7_E	27.3	9.4	18%	42%	10%	3.8
3UQ7_F	27.3	9.4	18%	42%	10%	3.8
3UQ7_G	27.3	9.4	18%	42%	10%	3.8
3UQ7_H	27.3	9.4	18%	42%	10%	3.8
3UQ7_I	27.3	9.4	18%	42%	10%	3.8
3UQ7_J	27.3	9.4	18%	42%	10%	3.8
3RIA_A	46.2	6.90E−06	22%	44%	4%	3.8
3RIA_B	46.2	6.90E−06	22%	44%	4%	3.8
3RIA_C	46.2	6.90E−06	22%	44%	4%	3.8
3RIA_D	46.2	6.90E−06	22%	44%	4%	3.8
3RIA_E	46.2	6.90E−06	22%	44%	4%	3.8
2BG9_B	176.4	1.20E−52	40%	65%	3%	4
2BG9_C	191.4	2.00E−58	42%	65%	5%	4
2BG9_A	192.6	7.00E−59	45%	63%	2%	4
2BG9_D	192.6	7.00E−59	45%	63%	2%	4
2BG9_E	199.1	2.60E−61	46%	67%	3%	4
3UQ5_A	27.3	9.4	18%	42%	10%	4.2
3UQ5_B	27.3	9.4	18%	42%	10%	4.2

Continued

3UQ5_C	27.3	9.4	18%	42%	10%	4.2
3UQ5_D	27.3	9.4	18%	42%	10%	4.2
3UQ5_E	27.3	9.4	18%	42%	10%	4.2
3UQ5_F	27.3	9.4	18%	42%	10%	4.2
3UQ5_G	27.3	9.4	18%	42%	10%	4.2
3UQ5_H	27.3	9.4	18%	42%	10%	4.2
3UQ5_I	27.3	9.4	18%	42%	10%	4.2
3UQ5_J	27.3	9.4	18%	42%	10%	4.2
1YI5_A	44.3	2.20E−05	24%	40%	3%	4.2
1YI5_B	44.3	2.20E−05	24%	40%	3%	4.2
1YI5_C	44.3	2.20E−05	24%	40%	3%	4.2
1YI5_D	44.3	2.20E−05	24%	40%	3%	4.2
1YI5_E	44.3	2.20E−05	24%	40%	3%	4.2
4AOE_A	57.4	2.90E−10	28%	49%	8%	5.8
4AOE_B	57.4	2.90E−10	28%	49%	8%	5.8
4AOE_C	57.4	2.90E−10	28%	49%	8%	5.8
4AOE_D	57.4	2.90E−10	28%	49%	8%	5.8
4AOE_E	57.4	2.90E−10	28%	49%	8%	5.8
4AOD_A	55.1	2.20E−09	24%	44%	6%	6
4AOD_B	55.1	2.20E−09	24%	44%	6%	6
4AOD_C	55.1	2.20E−09	24%	44%	6%	6
4AOD_D	55.1	2.20E−09	24%	44%	6%	6
4AOD_E	55.1	2.20E−09	24%	44%	6%	6
4AQ5_B	173.7	1.10E−50	39%	62%	5%	6.2
4AQ5_C	188.3	7.60E−56	39%	62%	7%	6.2
4AQ9_B	173.7	1.10E−50	39%	62%	5%	6.2
4AQ9_C	188.3	7.60E−56	39%	62%	7%	6.2
4AQ5_E	198.4	7.00E−60	44%	65%	6%	6.2
4AQ9_E	198.4	7.00E−60	44%	65%	6%	6.2
4AQ5_A	192.6	5.50E−58	45%	63%	2%	6.2
4AQ5_D	192.6	5.50E−58	45%	63%	2%	6.2
4AQ9_A	192.6	5.50E−58	45%	63%	2%	6.2
4AQ9_D	192.6	5.50E−58	45%	63%	2%	6.2

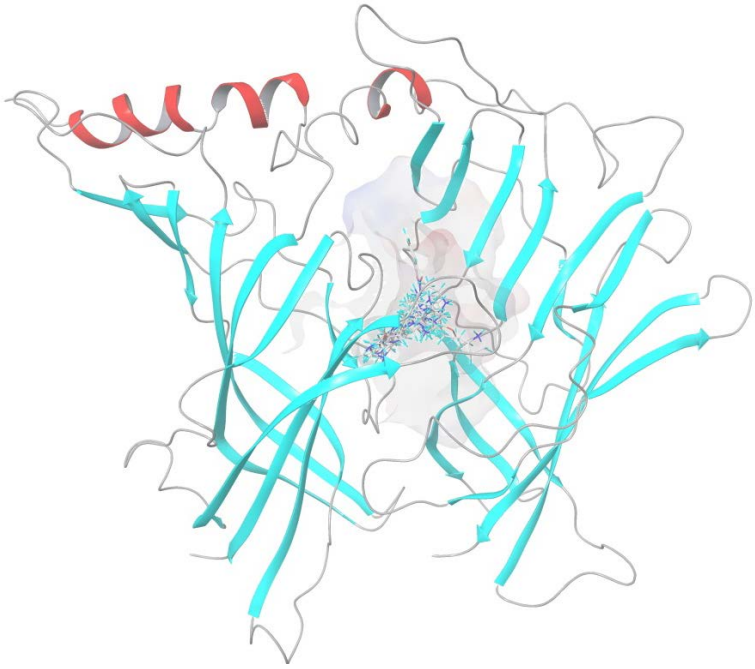

Figure S1. Docking poses of the 11 compounds in the homology model of human $\alpha 4\beta 2$ nACHR.